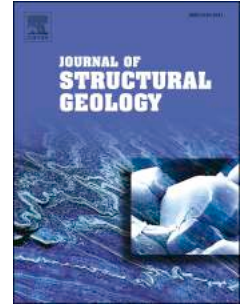


Accepted Manuscript

Emplacement of sandstone intrusions during contractional tectonics

Giuseppe Palladino, Antonio Grippa, Denis Bureau, G. Ian Alsop, Andrew Hurst



PII: S0191-8141(16)30086-4

DOI: [10.1016/j.jsg.2016.06.010](https://doi.org/10.1016/j.jsg.2016.06.010)

Reference: SG 3359

To appear in: *Journal of Structural Geology*

Received Date: 17 March 2016

Revised Date: 24 June 2016

Accepted Date: 29 June 2016

Please cite this article as: Palladino, G., Grippa, A., Bureau, D., Alsop, G.I., Hurst, A., Emplacement of sandstone intrusions during contractional tectonics, *Journal of Structural Geology* (2016), doi: 10.1016/j.jsg.2016.06.010.

This is a PDF file of an unedited manuscript that has been accepted for publication. As a service to our customers we are providing this early version of the manuscript. The manuscript will undergo copyediting, typesetting, and review of the resulting proof before it is published in its final form. Please note that during the production process errors may be discovered which could affect the content, and all legal disclaimers that apply to the journal pertain.

Emplacement of sandstone intrusions during contractional tectonics

Giuseppe Palladino^{a,*}, Antonio Grippa^a, Denis Bureau^b, G. Ian Alsop^a and Andrew Hurst^a

^aDepartment of Geology and Petroleum Geology, School of Geosciences, University of Aberdeen, Aberdeen, UK

^bBasin Studies Group, SEAES, University of Manchester, UK

Abstract

Sandstone injections are created by the forceful emplacement of remobilised sand in response to increases in overpressure. However, the contribution provided by horizontal compressive stress to the build-up in overpressure, and the resulting emplacement of sand injection complexes, is still to be substantiated by robust field observations. An opportunity to address this issue occurs in Central California where a large volume of sandstone intrusions record regionally-persistent supra-lithostatic pore-pressure. Detailed fieldwork allows sandstone-filled thrusts to be recognised and, for the first time, permits us to demonstrate that some sandstone intrusions are linked to contractional deformation affecting the western border of the Great Valley Basin. Fluidized sand was extensively injected along thrust surfaces, and also fills local dilatant cavities linked to thrusting. The main aims of this paper are to provide detailed descriptions of the newly recognized syn-tectonic injections, and describe detailed cross-cutting relationships with earlier sandstone injection complexes in the study area. Finally, an evolutionary model consisting of three phases of sand injection is provided. In this model, sand injection is linked to contractional tectonic episodes affecting the western side of the Great Valley Basin during the Early-Middle Cenozoic. This study demonstrates that sand injections, driven by fluid overpressure, may inject along thrusts and folds and thereby overcome stresses associated with regional contractional deformation. It is shown that different generations of sand injection can develop in the same area under the control of different stress regimes, linked to the evolving mountain chain.

Keywords: Sand injections, Contractional tectonics, Bed-parallel slip, Great Valley Sequence, San Joaquin Valley

30 1. Introduction

31 Large volumes of poorly consolidated sand, that are confined by sealing strata such as
32 mudstone, can be mobilized under the effect of increasing fluid overpressure and forcefully
33 injected into fractured host strata (e.g. Vigorito and Hurst, 2010). High pore-fluid pressure
34 required to cause sand injection (Hurst et al., 2011) may be controlled by mechanisms such as
35 depositional compaction, fluid volume change and fluid movement (Osborne and Swarbrick,
36 1997). Very little is known about sand injection generated by horizontal stress associated
37 with contractional deformation. This gap in knowledge is perhaps due to post-emplacement
38 overprinting processes linked to continuing contraction, and the expectation that contractional
39 deformation will tend to reduce space available to accommodate sandstone intrusions.
40 However, according to current models (e.g. Oliver, 1986; Ge and Garven, 1992; Lawrence
41 and Cornford, 1995), regional tectonic compaction results in a huge amount of groundwater
42 being expelled in major orogenic belts, thereby providing high pore fluid pressures that are
43 potentially able to drive sand injection (Fig.1). There are however, relatively few examples in
44 the published literature of sandstone intrusions being directly linked to contractional
45 tectonics. Winslow (1983) described clastic dike swarms formed of sandstone and
46 conglomerate that filled extensional fractures developed in the hangingwall of Cenozoic
47 thrusts in southern Chile. Other authors (Taylor, 1982; Di Tullio and Byrne, 1990; Ujiie,
48 1997) described sandstone intrusions filling contractional structures in southwest Japan,
49 while Phillips and Alsop (2000) suggest that sand may intrude both during and after regional
50 contractional deformation in the Caledonides of Scotland and Ireland.

51 In the western sector of the Great Valley Basin (Central California) (Fig. 2) large
52 exposures of sandstone intrusions in giant sand injection complexes are recognized at
53 different stratigraphic levels in the Great Valley Sequence. These sand injection complexes
54 suggest that multiple phases of rapid increases in pore-fluid pressure, recorded at basinal
55 scale, occurred during the Early Cenozoic. In particular, two independent giant sand injection
56 complexes, identified as the Panoche Giant Injection Complex (PGIC) and the Tumey Giant
57 Injection Complex (TGIC), formed in the Early Paleocene and Eocene respectively (Vigorito
58 et al., 2008; Hurst et al., 2011) (Fig. 3). As the emplacement of injection complexes occurred
59 in the undeformed sector of the basin, a direct link between sand injection and contractional
60 tectonics is not easy to demonstrate. However, earlier studies in Central California (Smyer
61 and Peterson, 1971) focussed on sand injections in the Early Paleocene complex and first
62 suggested a relationship between contractional tectonic activity and formation of sandstone

63 intrusions. Subsequent work conducted in the study area has mainly focussed on the
64 emplacement mechanisms, and the architectural organization, of sand injections (e.g. Jolly
65 and Lonergan, 2002; Vigorito and Hurst, 2010; Hurst et al., 2011; Scott et al., 2013), whereas
66 further structural investigations have not been undertaken. Recent fieldwork in the Panoche-
67 Tumey hills area in Central California (Fig. 2) allows the recognition of numerous examples
68 of well-preserved thrust and reverse faults filled by injected sand. The occurrence of these
69 syn-tectonic injections reveals for the first time the link between contractional deformation
70 observed in the study sector of Central California, and episodes of basin-scale injection. A
71 detailed description of the newly recognized syn-tectonic injections, analysis of the cross-
72 cutting relationships between sand injections belonging to the PGIC and TGIC complexes,
73 and the establishment of an evolutionary model for emplacement of giant sand injection
74 complexes are the main purposes of this paper.

75

76 **2. Geological setting**

77 *2.1 Regional setting*

78 The Panoche-Tumey hills area is located along the western margin of the San Joaquin Valley
79 (Central California) (Fig. 2a), which forms part of the Great Valley Basin (GVB). This is a
80 wide tectonic depression, positioned between the Franciscan accretionary complex and the
81 Sierran block, which is interpreted to be an emerged Meso-Cenozoic forearc basin (Ingersoll,
82 1979; Dickinson and Seely, 1979; Wakabayashi and Unruh, 1995; Constenius et al., 2000).
83 Here, an alternating series of major subsidence and shortening episodes occurred between the
84 Late Cretaceous and Early Cenozoic, and resulted in the deposition of a thick stratigraphic
85 sequence, punctuated by several sub-regional unconformities (Moxon, 1988). In the
86 Oligocene western North America switched from a convergent margin to the dextral strike-
87 slip San Andreas Fault Zone transform margin (Atwater and Stock, 1998; Sharman et al.,
88 2013), and the subsequent evolution of the area was essentially under the control of wrench
89 tectonics.

90 During the Quaternary, the GVB began a marked phase of uplift, which led to the
91 progressive emergence of the area that continues today (Page et al., 1998). The present
92 structural configuration of the eastern flank of the San Joaquin Basin (SJB) consists of an
93 extensive array of NW-SE trending en-échelon folds. The Tumey Hill Anticline, the

94 Vallecitos Syncline and the Coalinga Anticline are major folds in the area (Dibblee, 1981;
95 Bartow, 1991; Dickinson, 2002) (Fig. 2b). These structures are associated with many deep-
96 seated, double vergent thrusts and blind thrusts which display ramp-flat geometries when
97 imaged in seismic profiles (Namson and Davis, 1988). The study area consists of a NE-
98 dipping homocline forming the north-eastern flank of the Tumey Hill Anticline (Fig. 2c).
99 Here, the GVB infill consists of a thick accumulation of Jurassic to Quaternary marine and
100 non-marine clastic strata that unconformably overlie the Franciscan Complex (Fig. 3). It
101 mainly comprises two superimposed sedimentary series represented by the Great Valley
102 Sequence (GVS) (Bartow, 1996) and a Tertiary to Quaternary succession (TQS) respectively.

103

104 *2.2 Central California giant injection complexes*

105 Our study focuses on the Moreno and Kreyenhagen Shale formations that host the two giant
106 sand injection complexes, named the Panoche Giant Injection Complex (PGIC) and the
107 Tumey Giant Injection Complex (TGIC), (Vigorito et al., 2008; Hurst et al., 2011) (Fig. 3).
108 The PGIC is developed over an area of almost 400 km² and formed in response to a large-
109 scale supra-lithostatic pressure event in the Early Paleocene (Danian) (Schwartz et al., 2003;
110 Vigorito et al., 2008). The PGIC consists of a dike and sill network, intruded into the
111 mudstone-dominated Moreno Formation (Vigorito et al., 2008; Vigorito and Hurst, 2010;
112 Scott et al., 2013). Parent units for the injected sands of the PGIC consist of turbiditic
113 sandstones present in upper part of the Panoche Formation and in the lower part of the
114 Moreno Formation (Vigorito and Hurst, 2010).

115 The TGIC, which outcrops over an area of >500 km², was emplaced into Eocene
116 mudstones of the Kreyenhagen Shale (Huuse et al., 2004). Similar to the PGIC, the TGIC has
117 a complicated network of interconnected dikes and sills. It differs from the PGIC because of
118 the absence of extrudites and a paleo-seafloor, which if they existed, were removed by later
119 erosion; this unfortunately precludes constraining the precise timing of sand injection.
120 However, the TGIC intrudes Middle to Late Eocene Kreyenhagen Shale meaning that sand
121 injection cannot have occurred before the Middle Eocene. Furthermore, TGIC sandstone
122 intrusions are not present in the Miocene Temblor Formation above the unconformity,
123 therefore it is postulated that sand injection occurred before its deposition. The parent units of
124 the TGIC are uncertain, but Jenkins (1930) noted a similarity between the appearance of

125 sandstone in the TGIC and the Domengine Formation, which stratigraphically underlies the
126 Kreyenhagen Formation (Fig. 3).

127

128 **3. Sand injection and contractional deformation**

129 In the Panoche and Tumey hills fluidized sands were extensively injected along both thrust
130 surfaces and local dilatant cavities linked to the main contractional structures (Fig. 4). These
131 are recognized in the Moreno and the Kreyenhagen Shale formations and testify to a stage of
132 increasing overpressure and fluid migration related to contractional deformation. Details of
133 these structures from selected key outcrops (Fig. 2) are described below.

134

135 *3.1 Sand injection along thrust planes*

136 *3.1.1 Monocline Ridge 1 outcrop (MR1)*

137 Outcrop MR1 is located within the Monocline Ridge area (Fig. 2c) where the Kreyenhagen
138 Shale is deformed by a series of mesoscale sandstone-filled thrusts (Fig. 5). Two major
139 thrusts develop at different stratigraphic intervals (Figs. 5a, b). The upper structure (Box 1 in
140 Fig. 5b) shows a clear ramp-flat geometry where the bedding-parallel flat accommodates
141 shear along the detachment surface in the mudstone. To the north, this flat bifurcates into a
142 series of ramps marked by different inclinations. While sand is not observed to have injected
143 along the flat itself, it is intruded at the intersection point between ramps and flats and is also
144 present discontinuously along the ramps (Figs. 5a, b).

145 The lower structure (Box 2 in Fig. 5b) consists of an asymmetric fold, with an
146 overturned forelimb cored by two sandstone-filled blind thrusts (Figs. 5c, d). The main thrust
147 is filled with fine to medium-grained sand that progressively thins and dies out toward the
148 thrust tip. At the tip point, the thickness of the sandstone intrusion increases suddenly to form
149 a triangular geometry. Thickening is attributed to folding of the mudstone and the occurrence
150 of a 'saddle reef' in the fold hinge. A secondary thrust, which joins with the previously-
151 described structure, shows sandstone intrusions corresponding to a releasing step created
152 during thrust displacement. The recognized structures commonly consist of E-W oriented and
153 N-verging thrusts (Fig. 5e).

154

155 *3.1.2 Tumey Gulch 1 outcrop (TG1)*

156 Outcrop TG1 is located in Tumey Gulch (Fig. 2c) and comprises thinly-bedded turbidites of
157 the Moreno Formation. The outcrop contains a major SW-vergent thrust with an almost
158 undeformed hangingwall and a strongly deformed footwall (Fig. 6). Secondary thrust planes
159 and overturned folds are recognized. The major thrust plane develops along a 1 m-thick,
160 intensely fractured mudstone interval (Figs. 6a, b). In the hangingwall, bedding planes are
161 almost undeformed and sub-parallel to the thrust surface, or gently folded to form an open
162 anticline. In the footwall, minor thrust planes and tight, overturned drag folds accommodate
163 most of the deformation. Two major conjugate NW-SE and NE-SW striking sets of thrust
164 planes are present (Fig. 6c). Both sets are filled by sandstone intrusions (Fig. 6d, e), which
165 are easily distinguishable from depositional sandstones because of: i) the lack of primary
166 depositional structures, ii) the common occurrence of mudstone clasts eroded from the
167 surrounding host-strata, iii) the discordant geometry and irregular shape shown in cross-
168 section, and iv) their brown colour (that differs from the pale off-white depositional
169 sandstones). Sandstone intrusions are also more susceptible to weathering as they are very-
170 well sorted and therefore more permeable than the depositional sandstones. The close-
171 association between contractional structures and sandstone intrusions is apparent when
172 comparing dike attitudes (stereoplot 3 in Fig. 6c) with the orientations of thrust planes and
173 related folds (stereoplots 1 and 2 in Fig. 6c). Dikes display three preferential orientations,
174 with NW-SE and NE-SW trending dikes being consistent with the orientation of the main
175 thrusts, while N-S trending dikes form an earlier generation, which is cut by the thrusts
176 (detailed descriptions of these cross-cutting relationships are provided in section 4).

177

178 *3.1.3 Other significant outcrops*

179 Outcrops in the Silver Creek area (Fig. 2c) contain E to NE-vergent thrust planes
180 involving alternating thinly-bedded turbidites and mudstones of the Moreno Formation. In the
181 Silver Creek 1 outcrop (SC1) the main thrust surface exhibits a distinct ramp-flat geometry
182 (Fig. 7a, b). In the footwall of the flat segment, the beds are almost undeformed whereas in
183 the footwall of the ramp they form an overturned syncline. The beds are strongly deformed in
184 the hangingwall and a major frontal anticline occurs. The detachment surface mainly

185 develops in a 5 m thick mudstone where deformation is largely accommodated by mudstone
186 fracturing. However, where interbedded sandstone beds are present, additional minor thrust
187 planes, mesoscale asymmetrical folds and duplex structures are observed (Fig. 7c, d). Injected
188 sandstone is recognized both along the flat and ramp segments of the thrust surface. In the
189 thrust flat, they exploit structural discontinuities represented by bedding and horizontal
190 fractures, giving rise to roughly bed-parallel intrusions varying in thickness from 50 cm to 1.5
191 m. In thrust ramps, they are present along the oblique thrust surface, creating stepped
192 intrusions that show cross-cutting relationships with the host strata (Fig. 7e). Structural data
193 represented by NW-SE to N-S oriented sandstone-filled thrusts (see stereoplot in Fig. 7f)
194 indicate a constant top-to-the-E or NE sense of shear.

195 The Silver Creek 2 (SC2) outcrop (Fig. 8a) is located 700 m north of SC1 (Fig. 2c)
196 and displays a sharp thrust surface that separates an anticline/syncline fold pair. Beds
197 involved in the deformation consist of centimetres-to metres-thick remobilized depositional
198 sandstone, which locally retain their depositional structures such as lamination and normal
199 grading, despite being extensively fluidized. An older generation of dikes was also deformed
200 during this folding. Along the thrust surface, the sandstone intrusion is notably reduced in
201 thickness (maximum of 15 cm) compared to outcrop SC1 but is still visible cutting through
202 interbedded depositional sandstone and mudstone. Where the intrusion cuts through the
203 remobilized depositional sandstone, the contact between the intrusion and the depositional
204 sandstone is marked by contrasting colour, with white sandstone intrusions and orange
205 depositional sandstones. Similar to outcrop SC1, the sandstone-filled thrusts indicate a top-to-
206 the-E or NE sense of shear (stereoplot in Fig. 8b).

207 Further examples of sandstone-filled contractional structures occur in the Monocline
208 Ridge area (Fig. 2c) where sandstone intrusions cut through the Kreyenhagen Shale (Fig. 9a,
209 b). The Monocline Ridge 2 (MR2) outcrop exhibits a horizontally bedded section comprising
210 alternating dark and white mudstone and containing a set of dikes ranging in aperture from a
211 few centimetres to some decimetres. The dikes branch out from the underlying sandstone unit
212 which consists of a meter- thick, intensely remobilized, white turbiditic interval. Sand was
213 emplaced along bed-parallel discontinuities, and also two opposing NNE and SSW-facing
214 sets of thrust planes (with thrust facing following the definition of Lisle, 1985).

215

216 *3.2 Sand injection along dilational structures linked to contractional deformation*

217 Although thrust damage zones provide most of the accommodation space for syn-
218 contractional sandstone intrusions, other mechanisms associated with thrusting also
219 contribute to the creation of dilational space. In particular, additional accommodation is
220 obtained along bed-parallel dilatant fractures, dilational jogs, axial plane fractures and saddle
221 reefs in sedimentary multilayers (Ramsay, 1974; Sibson, 2005). Once filled by sandstone
222 intrusions, all these structures results in hinge-parallel fluid flow pathways.

223

224 *3.2.1 Bed-parallel dilatant fractures*

225 Sandstone-filled dilatant fractures are widely recognized in the study area forming
226 centimetres to metres-thick sandstone intrusions (Fig. 10a). These sandstone intrusions
227 approximate to bedding-parallel and form sills that display lensoid or sheet-like geometry.
228 Pinch-out terminations are very common. Detailed field observations reveal that fracture
229 opening typically favours sandstone/mudstone interfaces, although shaly partings in
230 mudstone can be exploited. Locally, different sandstone-filled bed-parallel dilatant fractures
231 are linked by horsetail extensional fractures (Kim et al., 2004) giving rise to stepped sills
232 (Fig. 10b). Dilatancy is created by hydraulic jacking caused by pore-fluid overpressure. The
233 sandstone intrusions are believed to develop parallel to stratigraphic and tectonic horizontal
234 discontinuities that are approximatively parallel to the local orientation of σ_1 during the
235 contractional tectonic stage.

236

237 *3.2.2 Dilational jogs*

238 Sandstone-filled dilational jogs are recognized in the footwall of a bed-parallel thrust
239 surface cutting through the Moreno Formation (Fig. 10c). These structures consist of a series
240 of lozenge-shaped sandstone intrusions that mainly develop parallel to the strike of the major
241 contractional structure. The direction of thrust displacement is determined from fold
242 asymmetry (Fig. 10c) and suggests a top-to-the ESE-E sense of shear. Dilational jogs (Fig.
243 10d) formed as Riedel structures (R') opened as a consequence of the progressive movement
244 of the fault (Fig. 10e). Another example of a sandstone-filled dilational jog is illustrated in
245 Fig. 10f, and shows a NE-verging reverse fault developed in the Kreyenhagen Shale. Fault
246 displacement is deduced by the offset of two marker sandstone horizons belonging to an

247 earlier sand injection complex. In this case, local dilatancy gave rise to a lozenge-shaped
248 cavity filled by injected sand (Fig. 10g).

249 In summary, dilational jogs occur in fault zones where the displacement vector is non-
250 parallel to fracture segments, and the result is an array of lozenge-shaped cavities with en-
251 échelon geometry. Fluidized sand filled these cavities instantaneously giving rise to tubular
252 strike-oriented bodies.

253

254 *3.2.3 Axial plane fracturing*

255 Sandstone-filled fractures are widely observed parallel to the axial planes of some of
256 the main folds recognized in the study area. These structures commonly consist of triangular-
257 shaped openings, which progressively taper downward toward the fold core (Fig. 10h). In the
258 Tumey Gulch area (Fig. 2c) where the Moreno succession is deformed into a roughly E-W
259 oriented anticline, the occurrence and orientation of sandstone dikes has been compared with
260 the orientation of fault and fracture planes associated with the folding (Fig. 10i). The similar
261 trends of the sandstone dikes with the major fold hinge, faults and fracture planes suggests
262 that sandstone intrusions are linked to the fold and fracture process (Fig. 10k). In summary,
263 axial plane fracturing is developed in the outer arcs of fold hinges and is interpreted to be
264 caused by outer-arc extension.

265

266 *3.2.4 Saddle reefs*

267 Saddle reefs consist of sandstone-filled dilational voids developed in the hinges of
268 folds. In the study area they are typically found in strongly-folded multi-layered strata at the
269 apex of chevron fold hinges considered to be formed by flexural slip (see Fig. 5c, d). Fluids
270 from more highly-pressured regions are interpreted to drain into the voids and, if sediment-
271 filled, may form almost continuous tubular bodies displaying small sectional areas but
272 extensive development along strike.

273

274 **4. Cross-cutting relationships**

275 Sandstone-filled thrusts show clear cross cutting relationships with their host strata and
276 earlier sandstone intrusions (Fig. 10f). In particular, dikes and sills belonging to the PGIC and
277 TGIC are systematically cut by sandstone-filled thrusts. Two styles of cross-cutting
278 relationships are observed (Fig. 11): i) primary cross-cutting relationships occur where
279 sandstone-filled contractional faults cut earlier dikes and sills. The sand intruded along the
280 fault plane is sourced by the fluidization of these earlier injections, suggesting they may be
281 easier to remobilize than adjacent depositional sandstones; ii) secondary cross-cutting
282 relationships occur where older generations of dikes are cut and segmented by flexural-slip
283 folding or bed-parallel shear during contractional tectonics. We now describe some examples
284 of primary and secondary cross-cutting relationships from key outcrops in the Moreno (PGIC)
285 and Kreyenhagen Shale (TGIC) formations.

286 The Monocline Ridge 3 (MR3) outcrop (Figs. 2c, 12a, b) consists of alternating
287 sandstone and mudstone belonging to the Kreyenhagen Shale that have been folded into a
288 decametric-scale open fold, which is repeatedly cut by two opposing NE and SW-facing sets
289 of thrust planes (Fig. 12c). Here, sandstone bodies consist of sandstone intrusions (sills and
290 dikes) pertaining to the TGIC and a few depositional sandstones. According to the criteria
291 proposed by Duranti and Hurst (2004), sills are recognized on the basis of erosional upper
292 surfaces, scattered mudstone clasts, and the lack of primary depositional structures. Syn-
293 contractional sandstone intrusions fill dilational jogs in reverse faults and thrusts and display
294 clear primary cross-cutting relationships with the older sills (Fig. 12d). Secondary cross-
295 cutting relationships are represented by dikes cut by flexural-slip surfaces (Fig. 12e).
296 Displacement occurs along the fold limbs in a direction that is opposed to the dip of the strata
297 (i.e. top towards the fold crest, c.f. Fossen, 2010).

298 The Monocline Ridge 4 (MR4) outcrop (Fig. 2c) consists of alternating thinly-bedded
299 marl, mudstone and sandstone of the Kreyenhagen Shale Formation (Fig. 13a, b) that are cut
300 by two opposing SW- and NW-facing sets of thrust planes (Fig. 13c). Most sandstone
301 consists of two different low-angle intrusive bodies, which slightly cross-cut bedding in the
302 host strata. The main structure is represented by a thrust surface dipping 45° SW, which
303 offsets the exposed succession by about 50 cm (based on the offset of the red-coloured
304 mudstone marker interval). Numerous secondary thrust planes showing well-preserved
305 slickensides are recognized (Fig. 13d, e). Cataclastic rocks formed by fragmented marl and
306 smeared mudstone are observed along the main thrust plane. In both the hangingwall and
307 footwall of the main thrust, the mudstone/marl host strata commonly maintain near-constant

308 thickness. Conversely, sandstone intervals show marked lateral thickness variations. In
309 particular, the sandstone intervals located in the footwall of the thrust are thin relative to their
310 hangingwall equivalents. It is hypothesized that when thrusting occurred, the unlithified
311 sandstone was fluidized and sand was contemporaneously injected along the thrust plane.

312 Notable examples of secondary cross-cutting relationships are widely observed in the
313 study area. Both well-exposed profile and strike-parallel sections allow a 3D view of these
314 structures. A profile-parallel section through dikes is exposed in Tumey Gulch (Fig. 2c). The
315 outcrop TG2 consists of a series of vertical or steeply inclined dikes with variable thickness
316 and attitude (Fig. 14a, b). Here, slip horizons are commonly developed along shaly laminae
317 or sandstone/mudstone interfaces. Along these surfaces, which may be marked by faint
318 slickensides, the dikes are offset with different amounts of displacement. In most cases, offset
319 occurs along sharp surfaces and the dikes affected are cut, but not otherwise deformed (Fig.
320 14c). In other cases offset dikes display deformational structures such as drag folds or
321 brecciation similar to examples shown by Becker et al. (1995). Locally, dike offsets appear to
322 be variable along the same shear surface however, this apparent discrepancy simply reflects
323 the fact that dikes are not parallel to one another, and form conjugate sets with different
324 orientations relative to slip (Fig. 14d).

325 A well-exposed strike-parallel section is observed in Dosados Canyon (DSC in Fig.
326 2c) where sub-vertical dikes have been laterally offset by flexural slip (Fig. 15a, b). In this
327 case, offset dike segments apparently diverge along the same shear surface from a
328 hypothetical vertical reference line located in the centre of the outcrop. This apparent
329 inconsistency is explained by the different attitude of the dikes which form a conjugate set
330 (stereoplots in Fig. 15c, d).

331 In summary, although dike segmentation occurs naturally during emplacement
332 (Delaney and Pollard, 1981), our observations provide further evidence that dikes can indeed
333 be cut by flexural slip (Borradaile, 1977; Taylor, 1982; Tanner, 1989; Becker et al., 1995), or
334 by coseismic slip during earthquakes (Weinberger et al., 2016).

335

336 5. Discussion

337 Recognition of sandstone-filled contractional structures in the PGIC and TGIC allows us to
338 deduce that at least three consecutive phases of sand injection occurred in the Panoche and

339 Tumey hills area during the early-middle Cenozoic. The emplacement of the first two
340 complexes appears not to have been directly controlled by contractional deformation,
341 although Smyers and Peterson (1971) recorded two sets of dikes filling a system of conjugate
342 shear fractures in the PGIC. These conjugates are consistent with a principal compressive
343 stress oriented approximately NNE-SSW in the study area. Conversely, the third phase of
344 sand injection, described for the first time in this paper, is strictly related to horizontal
345 contractional stress. Two fundamental questions arise: a) is the origin of sandstone-filled
346 contractional structures linked to regional tectonic deformation, or alternatively, is it related
347 to sedimentary processes associated with mass transport deposits (MTDs) within the San
348 Joaquin Basin?; b) which processes force fluidized sand to inject along the contractional
349 structures? We address these questions in the following section and then propose an
350 evolutionary model for sand injection in the study area.

351

352 *5.1 Origin of sand-filled contractional structures*

353 Folds and thrusts may originate in both tectonic and sedimentary environments as a result of
354 regional contraction, or slope failure associated with slumps and MTDs, and distinguishing
355 the origin of some structures may be problematic (e.g. Korneva et al., 2016). Sandstone
356 intrusions associated with contractional structures have been documented in both geological
357 contexts (Hiscott, 1979; Taylor, 1982; Winslow, 1983; Di Tullio and Byrne, 1990; Ujiie,
358 1997; Phillips and Alsop, 2000; Rowe et al., 2002; Odonne et al., 2011; Waldron and
359 Gagnon, 2011). In the case of slope failure associated with MTDs, the folds and faults that
360 record soft-sediment deformation are typical features characterizing the frontal parts of
361 slumps and submarine landslides in a variety of settings and lithologies (Martinsen and
362 Bakken, 1990; Smith, 2000; Strachan, 2002; Alsop and Marco, 2013; 2014; Alsop et al.,
363 2016; Jablonska et al., 2016). In order to determine if the origin of the sandstone-filled
364 contractional structures in the Panoche and Tumey hills area is sedimentary or tectonic, both
365 possibilities have been examined in the field. We propose a tectonic origin for these
366 sandstone-filled structures for the following reasons.

367

368 *5.1.1) Orientation of sandstone-filled contractional structures.*

369 The orientation of thrust planes and trends of fold axes measured show a dominant W-E to
370 NW-SE distribution (Fig. 16). This is consistent with the orientation of the main tectonic
371 structures observed at a regional scale (Aydin and Page, 1984; Bartow, 1991; Page et al.,
372 1998). Additionally, fold asymmetries and thrust vergence indicate a general top-to-the N or
373 NE sense of shear, although back-thrusts also occur locally. These shortening directions are
374 not consistent with the estimated orientation of the palaeoslopes measured in the Moreno and
375 Kreyenhagen Shale formations. According to McGuire (1988), Mitchell et al. (2010), and our
376 own data from the Moreno Formation, the paleocurrents indicate a predominant flow
377 direction toward the S and SW. Paleocurrent data collected in the Kreyenhagen Shale indicate
378 sediment transport toward the N and NW, which agrees with Clarke (1973) and Carter (1990)
379 (Fig. 16). Thus, the orientation of contractional structures supports regional tectonism rather
380 than downslope-driven MTDs.

381

382 *5.1.2) Cross-cutting relationships between sandstone injections and MTDs.*

383 Analysis of cross-cutting relationships shows that sandstone intrusions commonly cut through
384 gravity-induced deposits, for example slumps, within the Moreno Formation (Fig. 17). The
385 observation that sandstone intrusions post-date MTD emplacement suggests that slope failure
386 and sand injection episodes are neither genetically related nor concurrent.

387

388 *5.1.3) Fold geometry associated with sandstone-filled contractional structures.*

389 Analysis of fold geometry aids in the determination of the physical state of strata at the time
390 of deformation. According to Waldron and Gagnon (2011), deformation of sandstone layers
391 that display a near-parallel fold geometry, while adjacent mudstone interbeds are thickened in
392 the fold hinges, is related to tectonic deformation of lithified, competent strata. Conversely, if
393 mudstone layers display a parallel fold geometry and sandstone is typified by thickening in
394 the fold hinges, then folding is considered to have developed before significant lithification,
395 and relates to soft sediment deformation (Waldron and Gagnon, 2011). In the examples we
396 describe, sandstones display a near-parallel fold geometry whereas mudstone typically
397 displays thickening in fold hinges, suggesting that the former were at least not liquidized at
398 the time of deformation, and therefore were unlikely to have formed in a MTD.

399

400 *5.1.4) Brittle deformation associated with sandstone-filled contractional structures.*

401 Soft-sediment deformation occurs during the initial stages of sediment lithification and the
402 material involved in the deformation behaves in a ductile manner. However, in the examples
403 we describe, deformed strata clearly show evidence of brittle deformation. These include
404 intense fracturing affecting mudstone intervals along the main detachment surfaces, fold-
405 related cleavage, and the development of slickensides along the fault planes (Fig. 13e). The
406 recognition of brittle deformation generally supports a tectonic origin for the sandstone-filled
407 thrusts.

408

409 *5.1.5) Stratigraphic distribution of sandstone-filled contractional structures.*

410 Slumps and MTDs are generally restricted to particular stratigraphic intervals. Sandstone-
411 filled contractional structures however, cut through a number of different formations
412 pertaining to the Early Cenozoic GVB sequence and are geographically widespread. When
413 sandstone-filled contractional structures are observed within otherwise undeformed horizons,
414 deformation is related to bed-parallel shear mechanisms that affect the multi-layered
415 stratigraphic units in the PGIC and TGIC outcrop, which consist of thin-bedded sandstone
416 alternating with thinly-laminated mudstone. Widespread geographic distribution of
417 contractional structures and their occurrence in different lithostratigraphic units from the Late
418 Cretaceous to the Late Eocene support sand injection during regional tectonism, and render
419 emplacement of MTDs unlikely.

420

421 *5.1.6) Sedimentary associations of sandstone intrusions.*

422 The emplacement of large-scale MTDs is usually accompanied by the deposition of coarse-
423 grained deposits such as conglomerates, breccias, olistoliths, and blocks (see Sobiesiak et al.,
424 2016a, b). In the Moreno and Kreyenhagen Shale formations these coarse grained facies are
425 absent and only fine-grained turbidites with rare conglomeratic units present. The
426 sedimentary facies association thus supports sand injection along contractional structures
427 linked to regional tectonism rather than MTDs.

428

429 *5.2. Mechanisms driving emplacement of sand injections during contractional tectonics*

430 Fluidized sand is known to intrude through more than 1.5 km of overburden in the shallow
431 crust (Vigorito and Hurst, 2010). However, the emplacement of fluidised sand in
432 contractional settings is likely to be less favourable when compared to extensional settings
433 because of the adverse orientation of principal stresses. In contractional settings, a flat-lying
434 intrusive geometry is anticipated because σ_1 is horizontal and σ_3 vertical. Hence, intrusions
435 are not expected to emplace along thrust ramps where contractional deformation is
436 maximised. Our outcrop observations, together with a series of experimental models
437 investigating pluton emplacement along contractional structures (Galland et al., 2003; 2007;
438 Ferre' et al., 2012), demonstrate however, that intrusion along both the flat and ramp
439 segments of thrusts occur if contractional deformation and pore-fluid overpressure act in
440 concert. Laboratory experiments show that when injection occurs in a synthetic multilayer
441 medium characterized by the absence of contractional tectonics, conical or saucer-shaped
442 intrusions develop and propagate to the surface (Galland et al., 2003) (Fig. 18a). Similar
443 geometries are observed on outcrop and subsurface examples of sandstone intrusions where
444 there is no evidence that emplacement was influenced by contractional tectonics (Hurst and
445 Cartwright, 2007). Conversely, when contractional deformation is applied to a multilayer
446 medium the injection initially tends to form a flat-lying sill along the basal detachment
447 surface, and then propagates along thrust surfaces (Fig. 18b).

448 Although fluid overpressure is sustained in magmatic systems by the rise of hot
449 magma, the reasons for development of overpressure in sedimentary basins must be sought
450 within basin-scale processes. Various mechanisms have been proposed for the overpressuring
451 observed in the San Joaquin Valley (Wilson et al., 1999). Unusually high, near-lithostatic
452 fluid pressure is documented in hydrocarbon wells and springs distributed along the western
453 sector of the San Joaquin Valley and the adjacent Coast Range (Bredehoeft and Hanshaw,
454 1968; Lico and Kharaka, 1983) and there is a close similarity between present day
455 contractional structures and the distribution of observed overpressure in the Sacramento
456 Basin (McPherson and Garven, 1999). Based on field observations and numerical modelling
457 Berry (1973) and Unruh et al. (1992) attributed overpressure to contractional tectonic
458 processes, with other contemporaneous mechanisms such as sedimentary compaction,
459 diagenesis or hydrocarbon generation playing minor roles. According to these authors, crustal

460 shortening may have caused the rapid expulsion of fluids from compacting sandstone and
461 mudstone, thus increasing the overall pore-fluid pressure. Contemporaneously, the newly
462 formed tectonic discontinuities represented by thrust planes, reverse faults and fractures, may
463 have formed transient low-pressure zones, toward which almost instantaneous fluid migration
464 occurred, driven by a regional upward-directed pressure gradient.

465

466 *5.3. Possible post emplacement deformation*

467 Sandstone intrusions along thrust surfaces commonly appear discontinuous with irregular
468 geometries. The main reason for this is that sand was injected into tubular voids, which in
469 many cases are oriented parallel to the strike of contractional structures. This produces
470 lensoid geometries in transport-parallel cross sections. Another mechanism, represented by
471 later post-emplacement deformation, may also be responsible for the observed geometry.
472 Plastically deformed fragments of sandstone intrusions are frequently observed associated
473 with fault gouge. This suggests that poorly-lithified sandstone was involved in later fault
474 reactivation and that creep and ductile flow may have caused soft-sediment deformation.
475 Unfortunately, internal fabrics recognized in the sandstone intrusions do not allow to better
476 support this hypothesis, as they could have been generated either during sand fluidisation and
477 injection into open structural discontinuities, or later movement.

478

479 *5.4 Evolutionary model for emplacement of sandstone injections in the San Joaquin Valley*

480 In this study a late phase of sandstone-filled contractional structures that transect older sand
481 injection complexes, represented by the PGIC and TGIC, is recognised. Based on robust
482 geological outcrop evidence, an association is made between contractional tectonic events
483 and episodes of increased fluid pressure in the SJB. This hydrogeological association was
484 first suggested by Berry (1973) and subsequently confirmed by McPherson and Garven
485 (1999) based on the measurement of anomalous fluid pressures values in the Coast Range and
486 in the GVB. Our structural analysis, combined with the hydrogeological data, permits
487 reconstruction of a spatial and temporal evolutionary model consisting of three episodes of
488 high-pressure fluid flow along the western margin of the SJB during the Early Cenozoic (Fig.
489 19). The timing of emplacement of sand injection complexes is constrained in the study area
490 between the Early Paleocene to Oligocene and no sandstone intrusions are observed in

491 deposits younger than the Kreyenhagen Shale Formation. Stages of tectonic activity are
492 constrained by structural and stratigraphic frameworks (Nilsen, 1981; Rentschler and Bloch,
493 1988; Moxon, 1988; Bloch et al., 1993; Johnson and Graham, 2007).

494

495 *5.4.1. First sand injection event*

496 The first event (Fig. 19a) leading to the emplacement of the PGIC occurred during the
497 Danian, as testified by the extrusive complex recognized in the upper portion of the Moreno
498 Formation (Schwartz et al., 2003; Vigorito and Hurst, 2010). This emplacement coincided
499 with a major shortening episode marking the beginning of the Laramide orogeny that affected
500 the Great Valley Group and involved the eastward displacement of the Franciscan
501 accretionary complex during the Latest Maastrichtian to Early Paleocene (60–70 Ma)
502 (Wakabayashi and Unruh, 1995). The lack of sandstone-filled contractional structures in the
503 PGIC suggests that this portion of the basin was not directly involved in contractional
504 tectonics, and sandstone intrusions were predominantly emplaced along bedding planes and
505 open hydraulic-fractures. According to Smyers and Peterson (1971) a local control on
506 fracture distribution could have occurred due to the transmission of contractional stress from
507 the orogeny to the adjacent undeformed areas. The injection phase was followed by uplift and
508 subsequent subsidence as a consequence of eustatic sea level changes interacting with active
509 tectonism. The result was the deposition of two unconformity-bound, transgressive-regressive
510 cycles, represented by the Paleocene (Lodo Formation) and Early-Middle Eocene sequences
511 (Domengine Sandstone and Kreyenhagen Shale) (Almgren, 1984).

512

513 *5.4.2. Second sand injection event*

514 The second sand injection event occurred during or immediately after the deposition of the
515 Kreyenhagen Shale and gave rise to the TGIC (Fig. 19b). The study of the geometrical
516 organization of sandstone intrusions belonging to the TGIC reveals that at the time of
517 emplacement, the basin in which the Kreyenhagen Shale was deposited was unaffected by
518 contractional tectonics, and deposition occurred in a sector of the basin located distant from
519 the active chain. Similar to the PGIC, emplacement of sandstone intrusions occurred
520 predominantly along bedding surfaces and hydraulic fractures. In the proposed model, a
521 series of out-of-sequence thrusts is hypothesized to justify the general stratigraphic

522 transgressive trend shown by the Eocene units, and the build-up of fluid pressure responsible
523 for sand fluidisation, injection and formation of sandstone intrusions.

524

525 *5.4.3. Third sand injection event*

526 The third event (Fig. 19c) followed the emplacement of the TGIC as demonstrated by
527 the cross-cutting relationships (Figs. 12, 13). At this stage fluid migration occurred along
528 tectonic discontinuities, as shown by the sandstone-filled thrusts, rather than into hydraulic
529 fractures. During the Late Eocene the North American plate boundary switched from a
530 convergent to a transform margin but no outcrop observations can be directly and confidently
531 related to the final stages of plate convergence, or with the onset of the activity of the San
532 Andreas Fault. The injection event recorded in this study suggests a renewed stage of in-
533 sequence thrust advance and active involvement in the contractional deformation of areas
534 previously unaffected by tectonics.

535 Following the third sand injection event a widespread uplift stage took place in the
536 San Joaquin Basin. This uplift is recorded by a stratigraphic hiatus encompassing the Late
537 Eocene-Early Miocene, which is related to ongoing eustatic and tectonic factors (Moxon,
538 1988; Schulein, 1993). The erosion that followed resulted in the removal of the upper portion
539 of the Kreyenhagen Shale (and eventually other Eocene/Oligocene units), which is likely to
540 have hosted the upper part of the TGIC including the extrusive complex.

541 The correspondence between tectonic events and the build-up of fluid pressure in our
542 study area of the SJB is succinctly explained by the "squeegees" hydrological model
543 proposed to explain the generation and expulsion of water from orogenic belts (Oliver, 1986;
544 Qing and Mountjoy, 1992; Ge and Garven, 1992; Machel and Cavell, 1999; Bachu, 1999;
545 Ghiglione and Ramos, 2005). According to this hydrological model, pore space collapse
546 induced by tectonic compression results in a huge volume of water being expelled from
547 orogenic belts. The highly pressured groundwater can be driven upward toward the ocean
548 floor at the top of the accretionary wedge, or pushed laterally into the adjacent areas still not
549 affected by contractional deformation. Overpressured fluid migration may follow different
550 pathways, mainly represented by tectonic discontinuities and permeable stratigraphic levels.
551 We propose that the entry of overpressured groundwater into different sectors of the SJB
552 forearc unaffected by tectonic deformation, may have generated a hydraulic head that

553 triggered hydraulic fracturing and the sand fluidization necessary for the emplacement of the
554 PGIC and TGIC. Later, as the orogenic front encroached on the study area, tectonic
555 discontinuities became the preferred pathways for fluid flow, and sand was fluidised and
556 injected along contractional structures.

557

558 **6. Conclusions**

559 Sandstone intrusions emplaced along contractional structures marked by thrust and reverse
560 faults are recognized for the first time along the western margin of the San Joaquin Valley.
561 The sandstone intrusions form isolated bodies or swarms of sandstone dikes that cut through
562 the host mudstone and sandstone (either depositional or sandstone intrusions). The study of
563 cross-cutting relationships allows us to attribute the injection phase associated with
564 contractional tectonics to a late episode of injection, which cannot be older than Late Eocene.
565 This area of contraction-related injection is in an area where two previous giant injection
566 complexes formed and coincided with a crucial period in the tectonic evolution of the San
567 Joaquin Valley, as the western North American plate boundary switched from convergent to
568 the dextral strike-slip San Andreas Fault transform margin. It remains uncertain which of the
569 tectonic regimes exerted control over the emplacement of the sandstone intrusions. The
570 newly recognized sandstone intrusions are distributed over an area of at least 200 km² in the
571 Panoche and Tumey hills, and are developed in strata ranging in age from the Upper
572 Cretaceous to Middle Eocene. Their areal extent suggests a linkage of regionally-developed
573 overpressure to contractional tectonics. Consequently, an evolutionary model is proposed that
574 shows the relationships between the build-up of fluid pressure in the deformed chain and the
575 lateral transfer of the fluid that induces sand fluidization. The previously recognized sand
576 injection complexes (PGIC and TGIC) formed in an area still unaffected by contractional
577 tectonics, but were under the influence of fluid transferred toward them. During the final
578 phase of sand injection that is the focus of this study, contractional tectonics actively affected
579 the study area and is directly associated with the sand injection.

580

581 **Acknowledgments**

582 We acknowledge the support of sponsoring companies of Phase 3 of the Sand Injection
583 Research Group (SIRG). We are very grateful to John Waldron and Jessica Ross for the

584 constructive reviews of the manuscript. We also wish to thank and acknowledge the
585 continuing help and access provided by the Bureau of Land Management.

586

587 **References**

588 Almgren, A.A., 1984. Timing of submarine canyon and marine cycles of deposition in the
589 Southern Sacramento Valley, California. In Almgren A.A., Hacker P. D. (Eds.), Paleogene
590 submarine canyons of the Sacramento Valley, California: Pacific section, AAPG, 1-16.

591 Alsop G.I., Marco S., 2013. Seismogenic slump folds formed by gravity-driven tectonics
592 down a negligible subaqueous slope. *Tectonophysics* 605, 48–69.

593 Alsop G.I., Marco S., 2014. Fold and fabric relationships in temporally and spatially evolving
594 slump systems: A multi-cell flow model. *Journal of Structural Geology* 63, 27-49.

595 Alsop, G.I., Marco, S., Weinberger, R., Levi, T., 2016. Sedimentary and structural controls
596 on seismogenic slumping within mass transport deposits from the Dead Sea Basin.
597 *Sedimentary Geology*, doi: 10.1016/J.SEDGEO.2016.02.019 (in press).

598 Atwater, T., Stock, J., 1998. Pacific-North America Plate Tectonics of the Neogene
599 Southwestern United States: An Update. *International Geology Review* 40, 375-402.

600 Aydin, A., Page, B.M., 1984. Diverse Pliocene–Quaternary tectonics in a transform
601 environment, San Francisco Bay region, California. *Geological Society of America Bulletin*
602 95, 1303–1317.

603 Bachu, S., 1999. Flow systems in the Alberta Basin: Patterns, types and driving mechanisms.
604 *Bulletin of Canadian Petroleum Geology* 47, 455-474.

605 Bartow, J.A., 1991. The Cenozoic Evolution of the San Joaquin Valley California. USGS
606 Geological Survey Professional Paper, 1501, 40p.

607 Bartow, J.A., 1996. Geological Map of the West border of the San Joaquin Valley in the
608 Panoche Creek-Cantua Creek area, Fresno and San Benito Counties, California:
609 Miscellaneous Investigations Series-US Geological Survey Map I-2430, scale 1:50000.

- 610 Becker, A., Mazor, E., Becker, N., 1995. Flexural Slip in an Anticlinal Plungeout as a
611 Mechanism for Dike Offsets: Nahal Ardon Valley, Ramon National Geological Park, Israel.
612 *International Geology Review* 37, 601-622.
- 613 Berry, F.A.F., 1973. High fluid potentials in California Coast Ranges and their tectonic
614 significance. *AAPG Bulletin* 57, 1219–1249.
- 615 Bloch, R.B., Von Huene, R., Hart, P.E., Wentworth, C., 1993. Style and magnitude of
616 tectonic shortening normal to the San Andreas Fault across Pyramid Hills and Kettleman
617 Hills South Dome, California. *Geological Society of America Bulletin* 105, 464-478.
- 618 Borradaile, G.J., 1977. On cleavage and strain: results of a study in West Germany using
619 tectonically deformed sand dykes. *Geological Society [London]* 133, 146-164.
- 620 Bredehoeft, J.D., Hanshaw, B.B., 1968. On the maintenance of anomalous fluid pressures: 1.
621 Thick sedimentary sequences. *Geological Society of America Bulletin* 79, 1097-1106.
- 622 Carter, J.B., 1990. The Point of Rocks Sandstone, Temblor Range, California. In: *Structure,*
623 *Stratigraphy and Hydrocarbon Occurrences of the San Joaquin Basin, California (1990).*
624 *AAPG GB 65 and SEPM 64*, 331-337.
- 625 Clarke, S.H., 1973. The Eocene Point of Rocks Sandstone: Provenance, mode of deposition
626 and implications for the history of offset along the San Andreas Fault in central California.
627 Ph.D. thesis: Berkeley, California, University of California, 302 p.
- 628 Constenius, K.N., Johnson, R.A., Dickinson, W.R., Williams, T.A., 2000. Tectonic evolution
629 of the Jurassic–Cretaceous Great Valley forearc, California: Implications for the Franciscan
630 thrust-wedge hypothesis. *Geological Society of America Bulletin* 112, 1703–1723.
- 631 Delaney, P., Pollard, D.D., 1981. Deformation of host rocks and flow of magma during
632 growth of Minette dykes and breccia-bearing intrusions near Ship Rock, New Mexico. U.S:
633 *Geological Survey Professional Paper* 1202, 61p.
- 634 Dibblee, T.W., 1981. Regional Geology of the Central Diablo Range between Hollister and
635 New Idria. In *Geology of the Central and Northern Diablo Range. Annual meeting Pacific*
636 *Section Field trips 2 and 5. Society of Economic Palaeontologists and Mineralogists. Los*
637 *Angeles, California, USA*, 101-108.

- 638 Dickinson, W.R., Seely, D.R., 1979. Structure and stratigraphy of forearc regions. AAPG
639 Bulletin 63, 2–31.
- 640 Dickinson, W.R., 2002. Reappraisal of hypothetical Franciscan thrust wedging at Coalinga:
641 Implications for tectonic relations along the Great Valley flank of the California Coast
642 Ranges. *Tectonics*, 1039, doi: 10.1029/2001TC001315.
- 643 Di Tullio, L., Byrne, T., 1990. Deformation paths in the shallow levels of an accretionary
644 prism: The Eocene Shimanto belt of southwest Japan. *Geological Society of America*
645 *Bulletin* 102, 1420-1438.
- 646 Duranti, D., Hurst, A., 2004. Fluidization and injection in the deep-water sandstones of the
647 Eocene Alba Formation (UK North Sea). *Sedimentology* 51, 503–529.
- 648 Erslev, E.A., Mayborn, K.R., 1997. Multiple geometries and modes of fault-propagation
649 folding in the Canadian thrust belt. *Journal of Structural Geology* 19, 3-4, 321-335.
- 650 Ferre', E.C., Galland, O., Montanari, D., Kalakay, T.J., 2012. Granite magma migration and
651 emplacement along thrusts. *International Journal of Earth Sciences (Geologische*
652 *Rundschau)*, Springer, doi: 10.1007/s00531-012-0747-6.
- 653 Fossen, H., 2010. *Structural Geology. Redefining and classifying mélanges*. Cambridge
654 University Press, Cambridge, 480 p.
- 655 Galland, O., Cobbold, P.R., De Bremond d'Ars, J., Hallot, E., 2007. Rise and emplacement of
656 magma during horizontal shortening of the brittle crust: Insights from experimental
657 modelling. *Journal of Geophysical Research* 112, B06402, doi: 10.1029/2006JB004604.
- 658 Galland, O., De Bremond d'Ars, J., Cobbold, P.R., Hallot, E., 2003. Physical models of
659 magmatic intrusion during thrusting. *Terra Nova* 15, 405–409.
- 660 Ge, S., Garven, G., 1992. Hydromechanical modeling of tectonically driven groundwater
661 flow with application to the Arkoma Foreland Basin. *Journal of Geophysical Research* 97,
662 9119-9144.
- 663 Ghiglione, M.C., Ramos, V.A., 2005. Progression of deformation and sedimentation in the
664 southernmost Andes. *Tectonophysics* 405, 25-46.

- 665 Hiscott, R.N., 1979. Clastic sills and dikes associated with deep-water sandstones, Tourelle
666 Formation, Ordovician, Quebec. *Journal of Sedimentary Petrology* 49, 1-12.
- 667 Horne, R., Culshaw, N., 2001. Flexural slip folding in the Meguma Group, Nova Scotia,
668 Canada. *Journal of Structural Geology* 33, 1631-1652.
- 669 Hurst, A., Cartwright, J.A., 2007. Implications for Hydrocarbon Exploration and Production.
670 AAPG Memoir 87, Tulsa, 274 p.
- 671 Hurst, A., Scott, A., Vigorito, M., 2011. Physical characteristics of sand injectites: Earth-
672 Science Reviews 106, 215–246.
- 673 Huuse, M., Duranti, D., Steinsland, N., Guaranga, C.G., Prat, P., Holm, K., Cartwright, J.A.,
674 Hurst, A., 2004. Seismic characteristics of large-scale sandstones intrusions in the Paleogene
675 of the South Viking Graben, UK and Norwegian North Sea. In: Davies, R.J., Cartwright, J.A.,
676 Stewart, S.A., Lappin, M., Underhill, J.R. (Eds.), *Seismic technology: Application to the*
677 *Exploration of Sedimentary basins*. Geological Society, London Memoir 29, 263–277.
- 678 Ingersoll, R.V., 1979. Evolution of the Late Cretaceous forearc basin, northern and central
679 California. *Geological Society of America Bulletin* 90, 813-826.
- 680 Jablonska, D., Di Celma, C., Korneva, I., Tondi, E., Alsop, G.I., 2016. Mass-transport
681 deposits within basinal carbonates from southern Italy. *Italian Journal of Geosciences* 135,
682 30-40.
- 683 Jenkins, O.P., 1930. Sandstone dikes as conduits for oil migration through shales. *AAPG*
684 *Bulletin* 14, 411–421.
- 685 Jolly, R.J.H., Lonergan, L., 2002. Mechanisms and controls on the formation of sand
686 intrusions. *Journal of the Geological Society, London* 159, 605–617.
- 687 Johnson, C.L., Graham, S.A., 2007. Middle Tertiary Stratigraphic Sequences of the San
688 Joaquin Basin, California. In: *Petroleum systems and geologic assessment of oil and gas in*
689 *the San Joaquin Basin Province, California*. Hosford Scheirer, Allegra, Ed., 2007, U.S.
690 Geological Survey Professional Paper 1713.
- 691 Kim, Y., Peacock, D.C.P., Sanderson, D.J., 2004. Fault damage zones. *Journal of Structural*
692 *Geology* 26, 503–517.

- 693 Korneva, I., Tondi, E., Jablonska, D., Di Celma, C., Alsop, G.I., Agosta, F., 2016.
694 Distinguishing tectonically- and gravity-driven synsedimentary deformation structures along
695 the Apulian platform margin (Gargano promontory, southern Italy). *Marine and Petroleum*
696 *Geology* 73, 479-491, doi: 10.1016/j.marpetgeo.2015.12.009
- 697 Lawrence, S.R., Cornfordt, C., 1995. Basin geofluids. *Basin Research* 7, 1-7.
- 698 Lico, M.S., Kharaka, Y.K., 1983. Subsurface pressure and temperature distributions in
699 Sacramento Basin, California. *Selected Papers of the Pacific Section Annual Meeting* 1, 57-
700 75.
- 701 Lisle, R.J., 1985. The facing of faults. *Geological Magazine* 122, 249-251.
- 702 Machel, H.G., Cavell, P.A., 1999. Low-flux, tectonically-induced squeegee fluid flow ("hot
703 flash") into the Rocky Mountain Foreland Basin. *Bulletin of Canadian Petroleum Geology*
704 47, 510-533.
- 705 Martinsen, O.J, Bakken, B., 1990. Extensional and compressional zones in slumps and slides
706 in the Namurian of County Clare, Ireland. *Journal of the Geological Society, London* 147,
707 153-164.
- 708 McGuire, D.J., 1988. Stratigraphy, depositional history, and hydrocarbon source-rock
709 potential of the Upper Cretaceous-Lower Tertiary Moreno Formation, central San Joaquin
710 basin, California. PhD Thesis, Stanford University 231 pp.
- 711 McPherson, B.J.O.L., Garven, G., 1999. Hydrodynamics and overpressure mechanisms in the
712 Sacramento basin, California. *American Journal of Science* 299, 429-466.
- 713 Mitchell, C., Graham, S.A., Suck D.H., 2010. Subduction complex uplift and exhumation and
714 its influence on Maastrichtian forearc stratigraphy in the Great Valley Basin, northern San
715 Joaquin Valley, California. *Geological Society of America Bulletin* 122, 2063-2078, doi:
716 10.1130/B30180.1.
- 717 Moxon, I.W., 1988. Sequence stratigraphy of the Great Valley basin in the context of
718 convergent margin tectonics. In Graham, S.A., (Ed.), *Studies of the geology of the San*
719 *Joaquin Basin, Pacific Section. Society of Economic Paleontologists and Mineralogists* 60, 3-
720 28.

- 721 Namson, J.S., Davis, T.L., 1988. Seismically active fold and thrust belt in the San Joaquin
722 Valley, central California. *Geological Society of America Bulletin* 100, 257-273.
- 723 Nilsen, T.H., 1981. Early Cenozoic stratigraphy, tectonics, and sedimentation of the central
724 Diablo Range between Hollister and New Idria. In: Frizzell, V. (Ed.), *Geology of the central*
725 *Diablo Range, California. Field Trip Guidebook. Pacific Section SEPM, Los Angeles*, pp.
726 21–34.
- 727 Odonne, F., Callot, P., Debroas, E.J., Sempere, T., Hoareau, G., Maillard, A., 2011. Soft-
728 sediment deformation from submarine sliding: Favourable conditions and triggering
729 mechanisms in examples from the Eocene Sobrarbe delta (Ainsa, Spanish Pyrenees) and the
730 mid-Cretaceous Ayabacas Formation (Andes of Peru). *Sedimentary Geology* 235, 234–248.
- 731 Oliver, J. 1986. Fluids expelled tectonically from orogenic belts: Their role in hydrocarbon
732 migration and other geologic phenomena. *Geology* 14, 99-102.
- 733 Osborne, M.J., Swarbrick, R.E. 1997. Mechanisms for Generating Overpressure in
734 Sedimentary Basins: A Reevaluation. *AAPG Bulletin* 81, 1023–1041.
- 735 Page, B.M., Thompson, G.A., Coleman, R.G., 1998. Late Cenozoic tectonics of the central
736 and southern Coast Ranges of California: *Geological Society of America Bulletin*, 110, 846-
737 876.
- 738 Phillips, C.A., Alsop, G.I., 2000. Post-tectonic clastic dykes in the Dalradian of Scotland and
739 Ireland: implications for delayed lithification and deformation of sediments. *Geological*
740 *Journal* 35, 99-110.
- 741 Qing, H., Mountjoy, E.W., 1992. Large-scale fluid flow in the Middle Devonian Presqu'île
742 barrier, Western Canada Sedimentary Basin. *Geology* 20, 903-906.
- 743 Ramsay, J.G., 1974. Development of chevron folds: *Geological Society of America Bulletin*
744 85, 1741-1754.
- 745 Rentschler, M.S., Bloch, R.B., 1988. Flexural subsidence modelling of the Tertiary San
746 Joaquin Basin, California. In: *Studies of the Geology of the San Joaquin Basin*, Graham S.A.
747 (Ed.), Pacific Section, Society of Economic Paleontologists and Mineralogists, Los Angeles,
748 29-52.

- 749 Rowe, C.A., Mustard, P.S., Mahoney J.B., Katnick, D.C., 2002. Oriented Clastic Dike
750 Swarms as Indicators of Paleoslope? An Example from the Upper Cretaceous Nanaimo
751 Group, Canada. *Journal of Sedimentary Research* 72, 192–200.
- 752 Schulein, B.J., 1993. Sedimentation and tectonics of the upper lower to lower middle Eocene
753 Domengine Formation, Vallecitos syncline, California. M.S. thesis, Stanford University,
754 Stanford, California, 343 p.
- 755 Schwartz, H., Sample, J., Weberling, K.D. Minisini, D. Moore, J.C., 2003. An ancient linked
756 fluid migration system: cold-seep deposits and sandstone intrusions in the Panoche Hills,
757 California, USA. *Geo-Marine Letters* 23, 340–350, doi: 10.1007/s00367-003-0142-1.
- 758 Scott A., Hurst A., Vigorito M., 2013. Outcrop-based reservoir characterization of a
759 kilometer-scale sand-injectite complex. *AAPG Bulletin* 97, 309–343.
- 760 Sharman, G.R., Graham, S.A., Grove, M., Hourigan, J.K., 2013. A reappraisal of the early
761 slip history of the San Andreas fault, central California, USA. *Geology* 41, 727-730.
- 762 Sibson, R.H., 2005, Hinge-parallel fluid flow in fold-thrust belts: how widespread?.
763 *Proceedings of the Geologists Association* 116, 301-309.
- 764 Smith, J.V., 2000. Flow pattern within a Permian submarine slump recorded by oblique folds
765 and deformed fossils, Ulladulla, south-eastern Australia. *Sedimentology* 47, 357-366.
- 766 Smyers, N.B., Peterson, G.L., 1971. Sandstone Dikes and Sills in the Moreno Shale, Panoche
767 Hills, California. *Geological Society of America Bulletin* 82, 3201-3208.
- 768 Sobiesiak, M.S., Kneller, B., Alsop, G.I., Milana, J.P., 2016a. Inclusion of substrate blocks
769 within a mass transport deposit: a case study from Cerro Bola, Argentina. In: Lamarche, G.,
770 Mountjoy, J. (Eds.), *Submarine Mass Movements and their Consequences*. 487-496. Springer
771 International Publishing, Dordrecht.
- 772 Sobiesiak, M.S., Kneller, B., Alsop, G.I., Milana, J.P., 2016b. Internal deformation and
773 kinematic indicators within a tripartite mass transport deposit, NW Argentina. *Sedimentary*
774 *Geology*, doi: 10.1016/J.SEDGEO.2016.04.006 (in press).
- 775 Strachan, L.J., 2002. Slump-initiated and controlled syndepositional sandstone
776 remobilization: an example from the Namurian of County Clare, Ireland. *Sedimentology* 49,
777 25–41.

- 778 Tanner, G.P.W., 1989. The flexural-slip mechanism: *Journal of Structural Geology* 11, 635-
779 655.
- 780 Taylor, B.J., 1982. Sedimentary dykes, pipes and related structures in the mesozoic sediments
781 of south-eastern Alexander Island. *British Antarctic Survey Bulletin* 51, 1-42.
- 782 Ujiie, K., 1997. Off-scraping accretionary process under the subduction of young oceanic
783 crust: The Shimanto Belt of Okinawa Island, Ryukyu Arc. *Tectonics* 16, 305-322.
- 784 Unruh, J.R., Davisson, M.L., Criss, R.E., Moores E.M., 1992. Implications of perennial saline
785 springs for abnormally high fluid pressures and active thrusting in western California.
786 *Geology* 20, 431-434.
- 787 Vigorito, M., Hurst, A., Cartwright, J., Scott, A., 2008. Regional-scale shallow crustal
788 remobilization: processes and architecture. Geological Society [London] Special Publication
789 165, 609–612.
- 790 Vigorito, M., Hurst, A., 2010. Regional sand injectite architecture as a record of pore
791 pressure evolution and sand redistribution in the shallow crust: insights from the Panoche
792 Giant Injection Complex, California. *Journal of the Geological Society [London]* 167, 889–
793 904.
- 794 Wakabayashi J., Unruh J.R., 1995. Tectonic wedging, blueschist metamorphism, and
795 exposure of blueschists: Are they compatible?. *Geology* 23, 85-88.
- 796 Waldron, J.W.F., Gagnon, J.F., 2011. Recognizing soft-sediment structures in deformed
797 rocks of orogens. *Journal of Structural Geology* 33, 271-279.
- 798 Weinberger, R., Levi, T., Alsop, G.I., Eyal, Y., 2016. Coseismic horizontal slip revealed by
799 sheared clastic dikes in the Dead Sea Basin. *Geological Society of America Bulletin*, 128,
800 1193-1206. doi: 10.1130/B31415.1
- 801 Winslow, M.A., 1983. Clastic dike swarms and the structural evolution of the foreland fold
802 and thrust belt of the southern Andes. *Geological Society of America Bulletin* 94, 1073-1080.
- 803 Wilson, M.A., Garven, G., Boles, J.R., 1999. Paleohydrogeology of the San Joaquin basin,
804 California. *Geological Society of America Bulletin* 111, 432–449.
- 805

806 **Figure captions**

807 **Fig. 1.** Simplified model showing the main fluid migration pathways in an orogenic belt
808 (after Oliver, 1986). A huge amount of water is generated and then expelled because of
809 contractional deformation in thrust and fold belts. Hpp: high pore-pressure; Lpp: low pore-
810 pressure.

811

812 **Fig. 2.** a) Location of the study area in California with the San Andreas Fault Zone (SAFZ)
813 shown in red. b) Geological map of the western margin of the San Joaquin Valley showing
814 the main structures recognized. The red box defines the study area. c) Geological map of the
815 study area with the relevant stratigraphic units (modified from Bartow, 1996). Outcrop
816 locations are also shown.

817

818 **Fig. 3.** Stratigraphic column showing the geological units cropping out in the Panoche and
819 Tumey hills (modified from Bartow, 1996). The stratigraphic position of the giant sand
820 injection complexes is marked. GVS-Great Valley Sequence; TQS-Tertiary to Quaternary
821 Sequence; PGIC-Panoche Giant Injection Complex; TGIC-Tumey Giant Injection Complex.

822

823 **Fig. 4.** Simplified model showing the distribution of fluidized sand in a thrust (modified from
824 Erslev and Mayborn, 1997). Intrusions preferentially occur along the thrust surface, and also
825 in dilatant cavities in the hangingwall and footwall of the thrust.

826

827 **Fig. 5.** a) Photograph and b) associated line drawing of outcrop MR1 ($36^{\circ}30.709'N$ 120°
828 $32.989'W$) showing two stacked N-verging sandstone-filled thrusts (in boxes). c) Photograph
829 and d) associated line drawing showing detail of the blind sandstone-filled thrust from 5a.
830 Note that the offset across the thrust progressively decreases toward the tip of the intrusion. e)
831 Lower hemisphere stereoplot showing the orientation of the thrust planes (great circles).

832

833 **Fig. 6.** a) Photograph and b) associated line drawing of outcrop at Tumey Gulch (TG1) (36°
834 31.215°N $120^{\circ} 38.407^{\circ}\text{W}$) showing a SW-verging thrust filled by sandstone intrusions. c)
835 Equal area lower hemisphere stereoplots showing two different thrust trends visible on
836 stereoplot 1. Contoured fold hinges are shown in stereoplot 2, while dike orientations
837 (stereoplot 3) display a similar orientation to the trend of the thrusts. d) and e) Details of the
838 sandstone-filled thrust (see Figure 6b), note that the sandstone intrusion initially follows
839 bedding planes and then turns abruptly to intrude along the thrust surface.

840

841 **Fig. 7.** a) Photograph (person for scale in the circle) and b) associated line drawing of outcrop
842 at Silver Creek (SC1). c, d) Minor contractional structures recognized along the flat segment
843 of the thrust. In this sector the development of meso-scale fold and duplexes is favoured by
844 the occurrence of thin-bedded depositional sandstones. e) Stepped sandstone intrusion
845 recognized along the thrust ramp shear zone. The underlying sandstone consists of strongly
846 deformed and remobilized depositional units. f) Equal area (lower hemisphere) stereoplot
847 showing the main thrust trends present.

848

849 **Fig. 8.** a) Outcrop at Silver Creek (SC2) showing white-coloured sandstone intruded along
850 the thrust surface. Note that the pre-existing dike was deformed during limb rotation of the
851 hangingwall anticline. b) Equal area (lower hemisphere) stereoplot showing the orientation of
852 the main thrust planes.

853

854 **Fig. 9.** a) Photograph and b) associated line drawing of outcrop at Monocline Ridge (MR2)
855 showing a double vergent NNE-SSW trending sandstone-filled fault system cutting through a
856 thin-bedded section of mudstone. Sand was sourced from the underlying unit, which is a
857 depositional unit strongly remobilized during fluidisation.

858

859 **Fig. 10.** Sandstone-filled dilational structures associated with contractional deformation. a)
860 Bed-parallel sandstone intrusions and b) associated line drawing from Dosados Canyon. Note
861 that the two main horizontal intrusions are connected by oblique horsetail structures. These
862 structures indicate that the opening of the fractures was not purely vertical but was

863 accomplished by dextral bed-parallel shear (red arrows). c) Lozenge-shaped dilational jogs in
864 the footwall of a bed-parallel shear surface at Right Angle Canyon. An asymmetric folded
865 sandstone bed visible in the hangingwall provides a sense of shear consistent with the
866 opening of dilational jogs. d) Detail of Fig. 10c. e) Dilational jogs opened along R' fractures
867 as shown in the model. f) Sandstone-filled releasing step recognized along a NW-SE trending
868 reverse fault in Monocline Ridge. Fault kinematics is constrained by offset marker layers and
869 by fault gouge. g) Detail of Fig. 10f. h) An E-W trending sandstone-filled extensional fault
870 recognized in the Tumey Hill area. Comparison between i) the major fold axes and k) faults,
871 fractures, and dikes trends recognized at Tumey Hill.

872

873 **Fig. 11.** Diagram showing primary and secondary cross-cutting relationships as recognized in
874 the Panoche and Tumey hills area.

875

876 **Fig. 12.** a) Photograph and b) associated line drawing of the outcrop Monocline Ridge (MR3)
877 ($36^{\circ} 32.023' N 120^{\circ} 33.827' W$) showing deformed TGIC dikes and sills. c) Equal area
878 (lower hemisphere) stereoplots showing NW-SE trending thrust planes as great circles and
879 contoured poles to thrust planes. d) Primary cross-cutting relationships represented by a syn-
880 contractional reverse fault that cuts a pre-existing sill (position shown in Fig. 12b). Note that
881 syn-contractional sandstone intrusion only occurs where dilational jogs formed along the
882 fault plane. e) Details of sandstone dikes showing secondary cross-cutting relationships.
883 Displacement occurs along the fold limbs in a direction opposed to the dip of the strata (i.e.
884 top toward the fold crest).

885

886 **Fig. 13.** a) Photograph and b) associated line drawing of the outcrop Monocline Ridge
887 (MR4). Note the lateral thickness variation characterizing the sandstone intrusions cut by the
888 major thrust plane with sand injected along the thrust surface. c) Equal area (lower
889 hemisphere) stereoplot showing the orientation of the main thrust planes. d) Detail of a
890 secondary thrust plane associated with the major structure. e) Striation recognized along a
891 secondary thrust surface associated with the major structure. The length of the ruler is 10 cm.

892

893 **Fig. 14.** a) A profile-parallel section exposure showing a set of conjugate dikes cut by
894 flexural slip in Tumey Gulch. Lateral offset varies from a few centimetres to several
895 decimetres. The prevalent movement direction is toward the NE. b) Interpretation showing
896 the prevalent slip vectors (highlighted by red arrows). c) Detail of Fig. 14a showing the main
897 dike which is cut by a flexural slip surface. d) Stereoplots showing orientations of the dikes.
898 Multiple great circles on some stereoplots represent the different segments of a single dike.

899

900 **Fig. 15.** a) An along strike-parallel section showing a set of dikes cut by flexural slip,
901 Dosados Canyon. b) Interpretation showing the apparent slip vectors (red arrows). Based on
902 bedding and dike attitudes, the movement direction of the different rock packages is toward
903 the viewer (in the third dimension). Note that bedding-parallel intrusions occurred along the
904 major slip horizons, which most likely formed during flexural slip. c) Stereoplots showing
905 bedding and dike attitudes. Multiple great circles depicted by some stereoplots represent
906 different segments of a single dike. d) A schematic diagram showing the relationships
907 between the direction of flexural slip and offset of conjugate dikes (modified from Horne and
908 Culshaw, 2001).

909

910 **Fig. 16.** Simplified geological and structural map of the Panoche and Tumey hills area. The
911 stereoplots (equal-area, lower hemisphere) summarize the orientations of thrusts and reverse
912 faults. Black arrows indicate the directions of PGIC and TGIC paleocurrent data measured in
913 the field. The dominant W-E to NW-SE strikes and the general top-to-the N or NE sense of
914 shear shown by thrust planes is consistent with the main tectonic structures present at
915 regional scale.

916

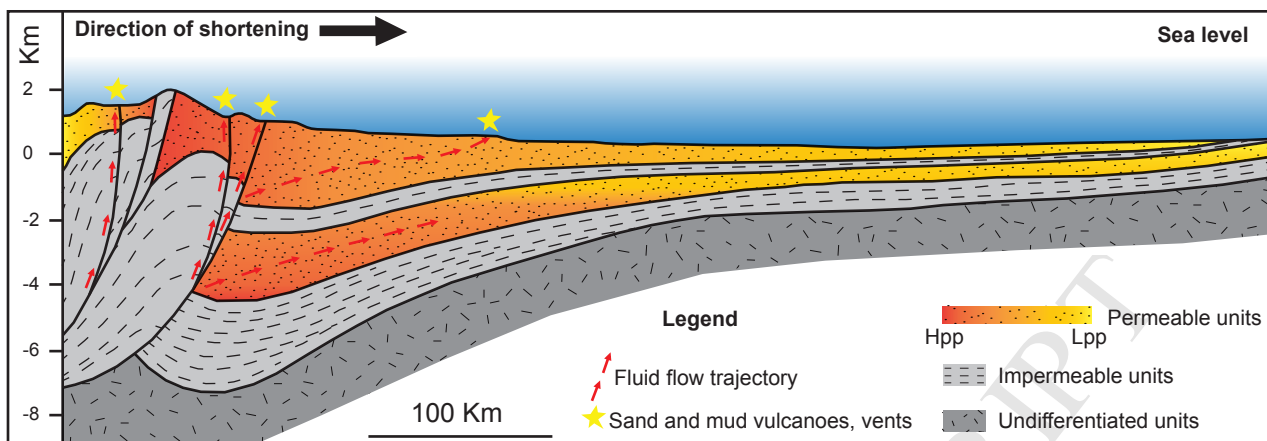
917 **Fig. 17.** Cross-cutting relationships between sandstone intrusions and MTDs observed in
918 West Tumey. In this outcrop a slump interval is clearly cut by two dikes (1 and 2). The
919 visible offset in the slump interval across sand injections is related to jack-up (white arrow)
920 produced during emplacement of the underlying sill.

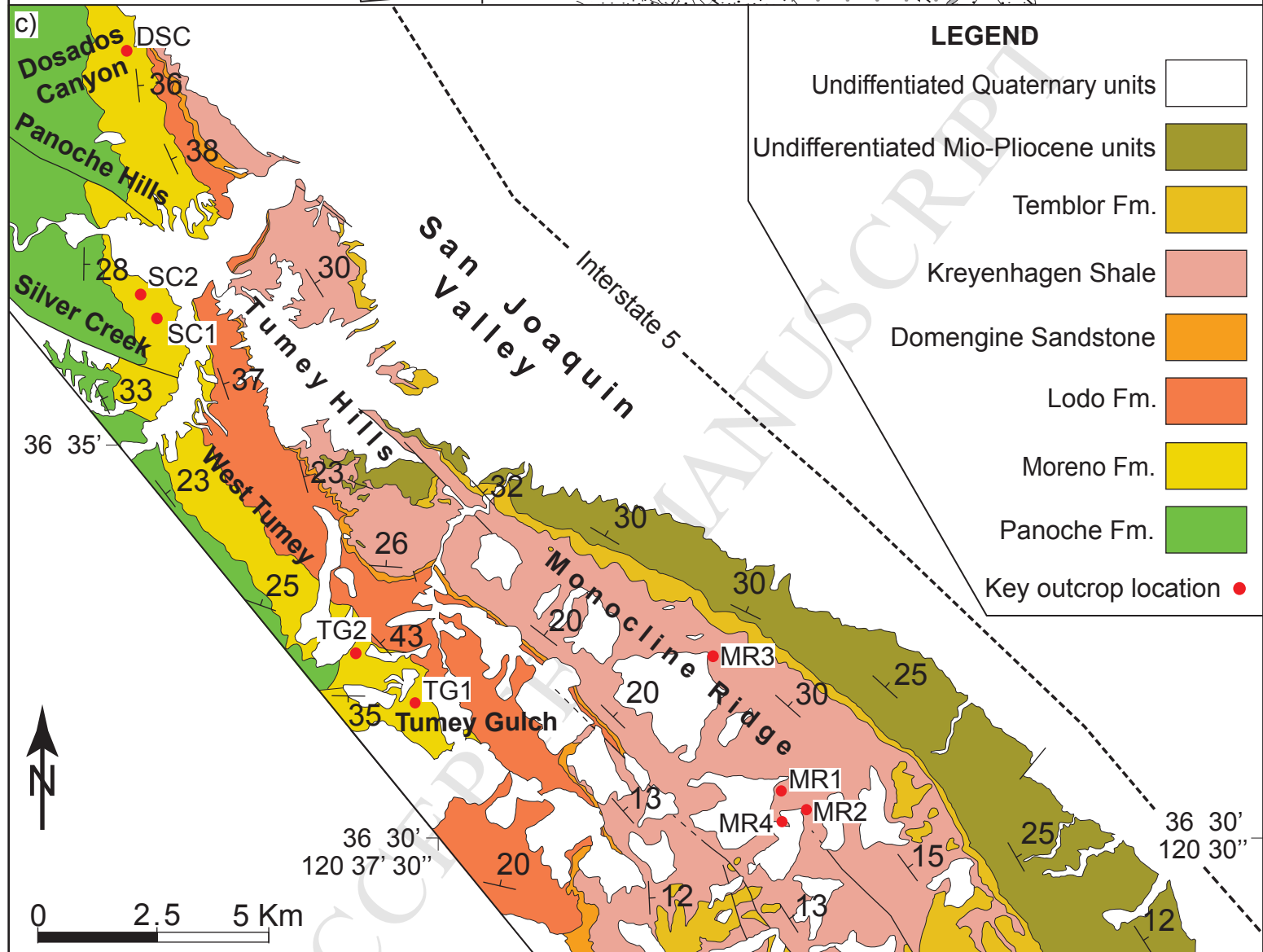
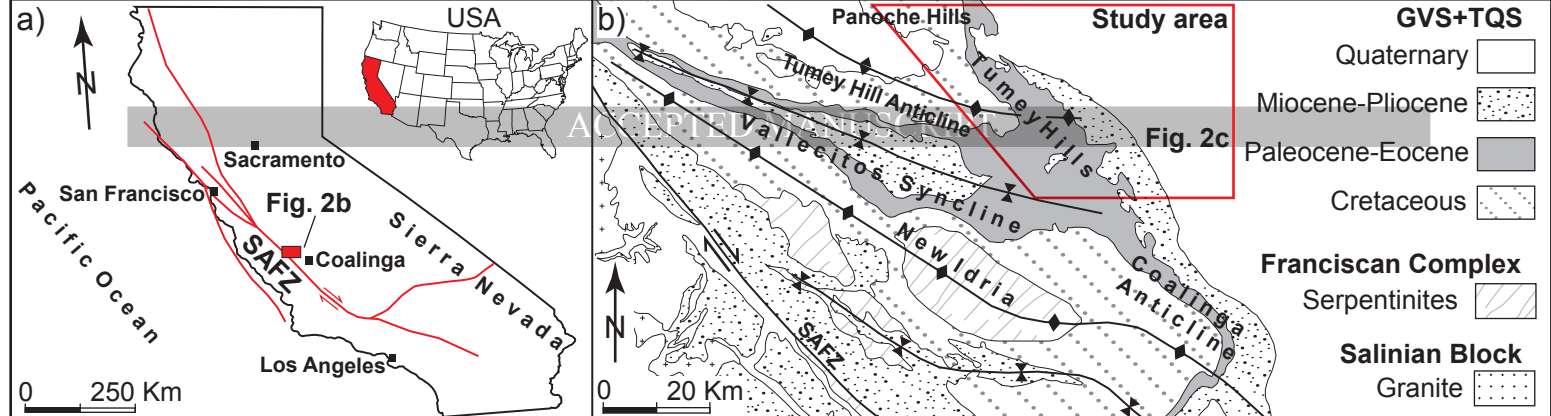
921

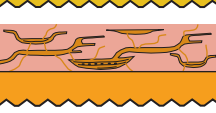


922 **Fig. 18.** Summary of results of the laboratory experiments conducted by Galland et al.
923 (2003). a) Without horizontal compression, injection of vegetable oil in powdered silica
924 resulted in a saucer-shaped intrusion. b) Applying horizontal stress, vegetable oil injected
925 along the thrust surface and thickened at the core of the anticlines to produce saddle reefs.
926 Note the strong similarity between these experimental geometries and the sandstone
927 intrusions shown in Fig. 5c, d.

928

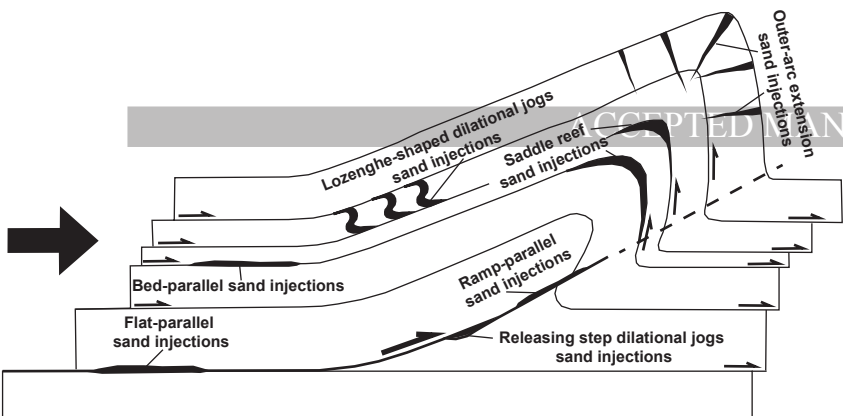
929 **Fig. 19.** Diagrams showing the proposed evolutionary model for the emplacement of
930 sandstone intrusions in the study area of the San Joaquin Valley during Early-Middle
931 Cenozoic (thickness of the different units not to scale). a) Emplacement of PGIC during the
932 Danian in the upper portion of the Moreno Formation at the beginning of the Laramide
933 orogeny. b) Emplacement of the TGIC during Middle-Upper Eocene. c) Emplacement of
934 sand-filled thrusts during Late Eocene-Oligocene when the study area was directly affected
935 by contractional tectonics. Fluid migration occurred along tectonic discontinuities leading to
936 the emplacement of the sandstone-filled thrusts. Hpp: high pore-pressure; Lpp: low pore-
937 pressure.



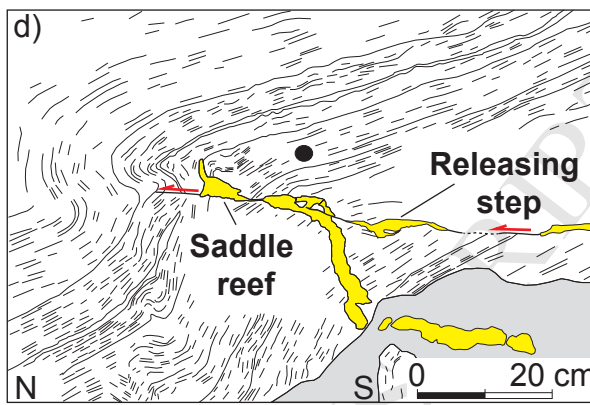
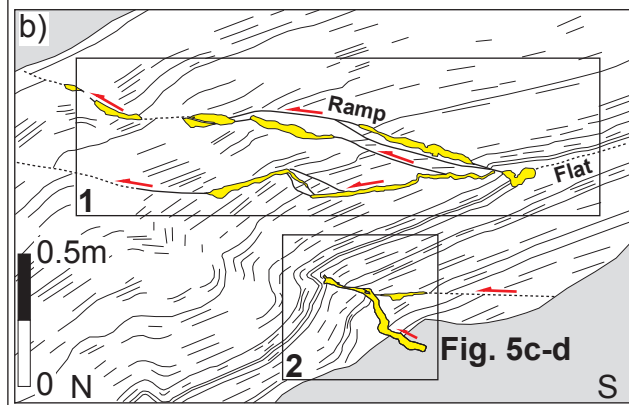
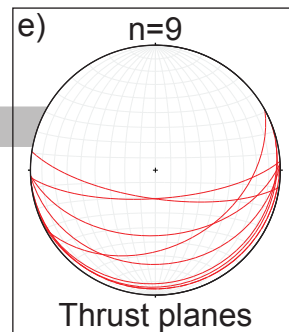


Age		Stratig. Sequence	Formation	Injection Complex
Plei. / Ho.		Tertiary-Quaternary Sequence (TQS)	Undifferentiated Quaternary units	Tumey Giant Injection Complex (TGIC)
Pli.			Undifferentiated Mio-Pliocene units	
Mioc.			Temblor Fm.	
Oli.			Kreyenhagen Shale	
Eoc.			Domengine Sandstone	
Pal.		Lodo Fm.		
Cretac.		Great Valley Sequence (GVS)	Moreno Fm.	Panoche Giant Injection Complex (PGIC)
			Panoche Fm.	

ACCEPTED MANUSCRIPT



ACCEPTED MANUSCRIPT



Cover

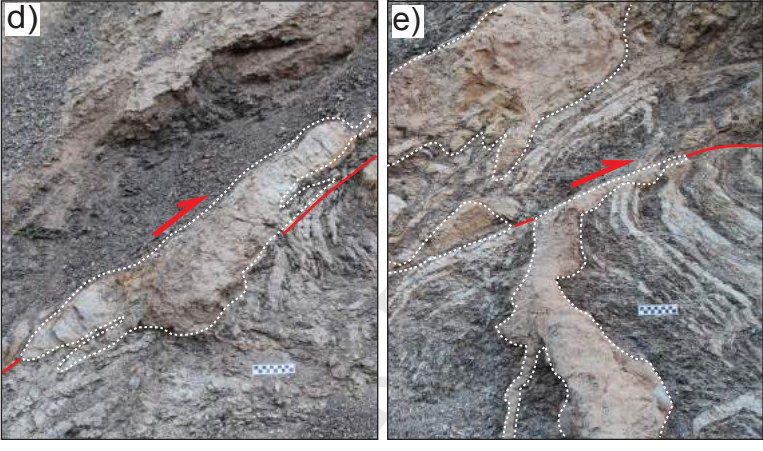
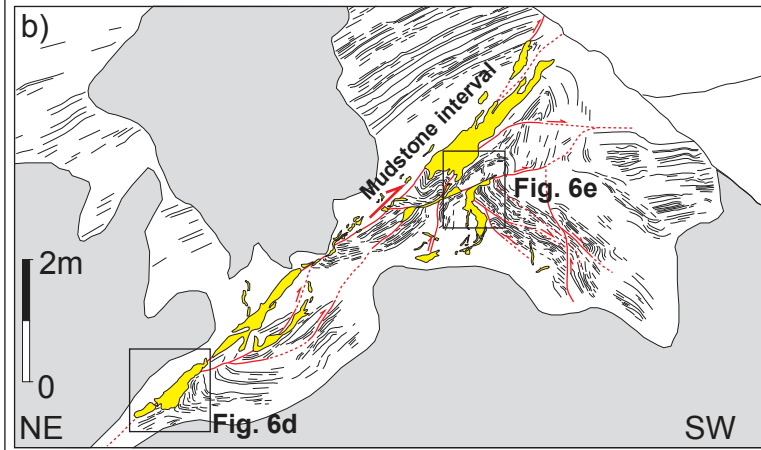
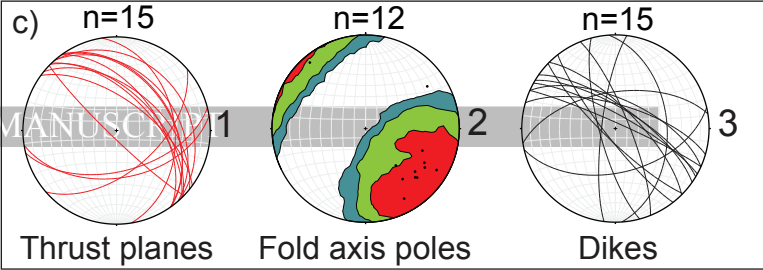


Injected sandstone

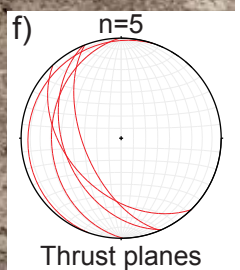
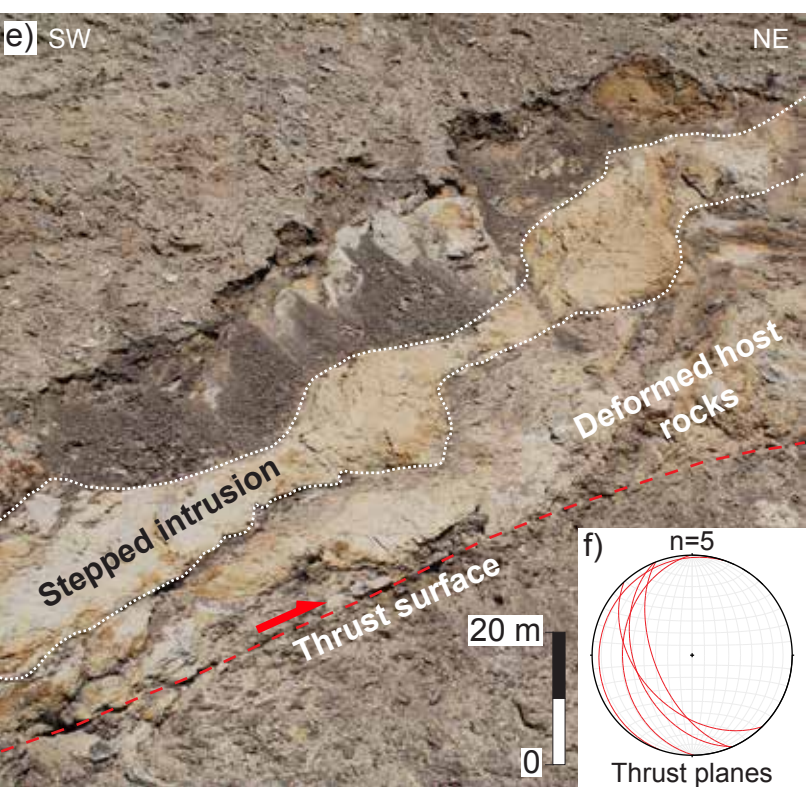
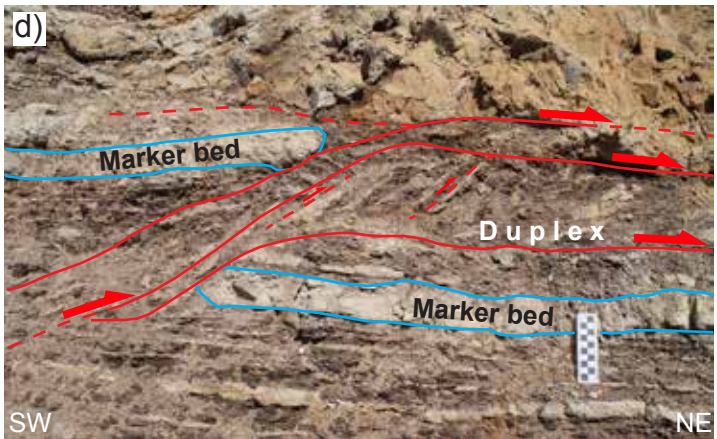
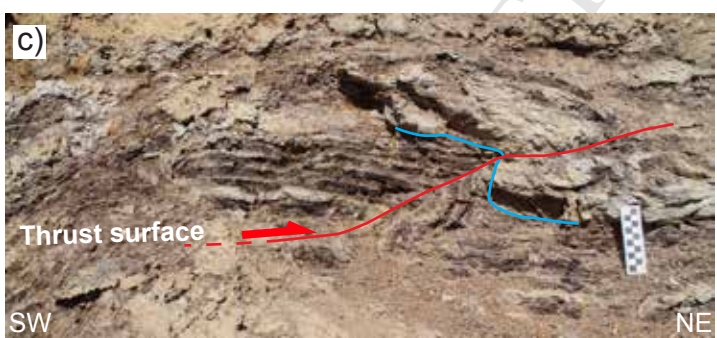
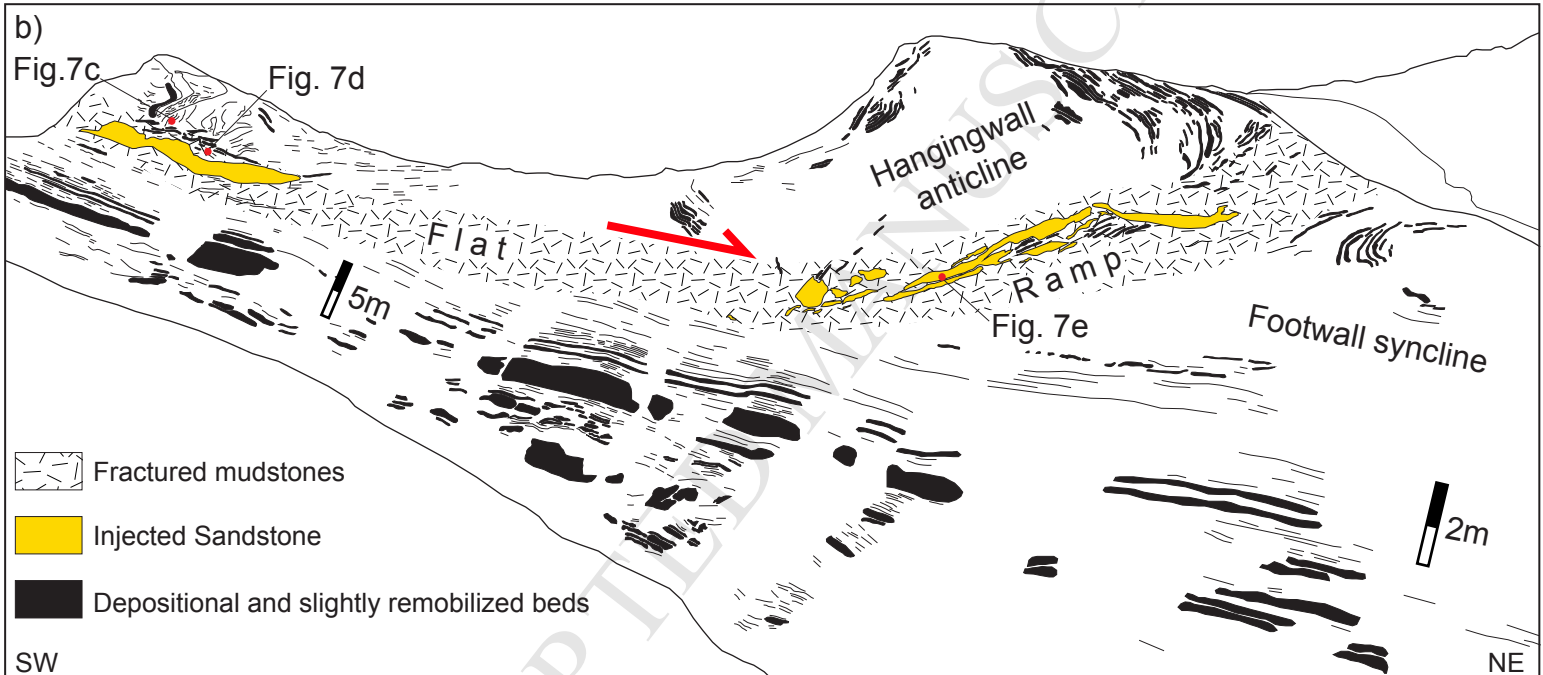


mudstone

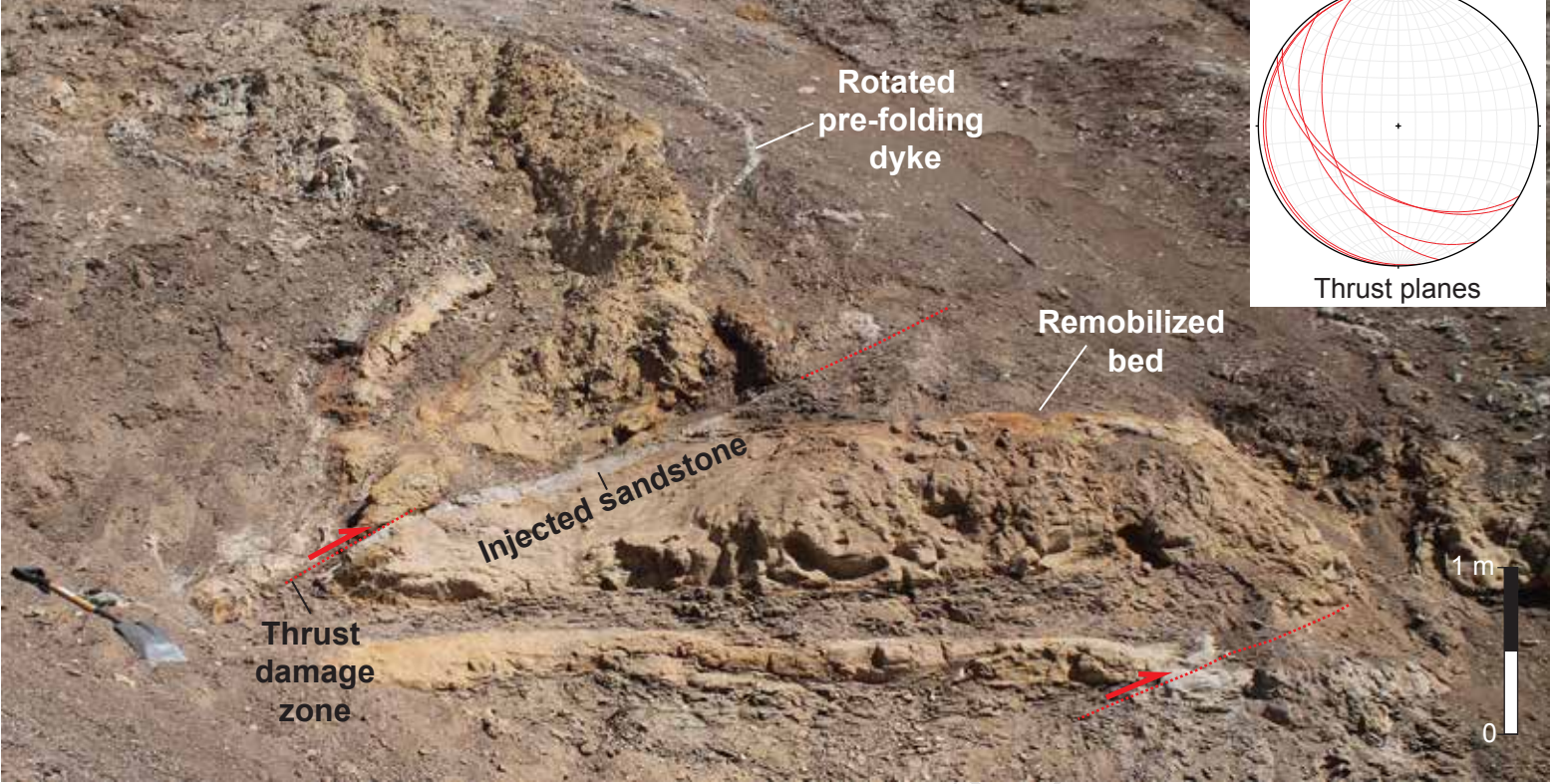
ACCEPTED MANUSCRIPT



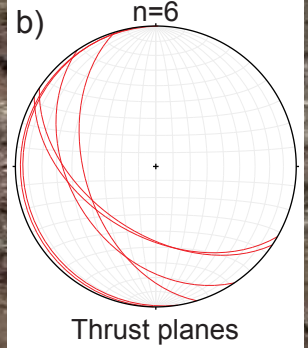
ACCEPTED MANUSCRIPT



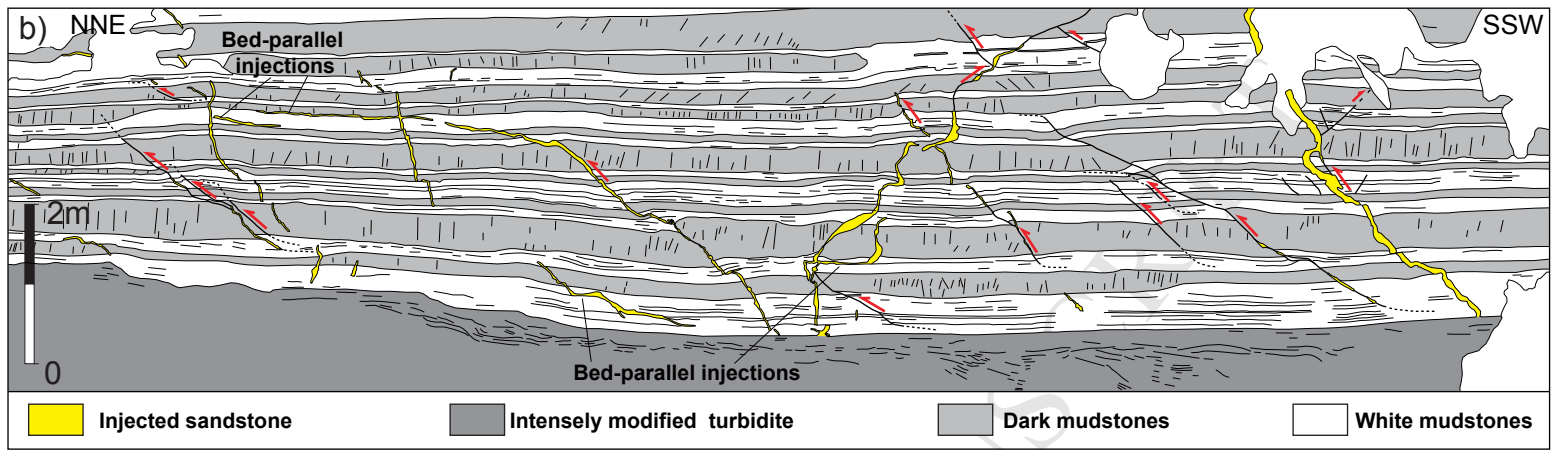
a) WNW



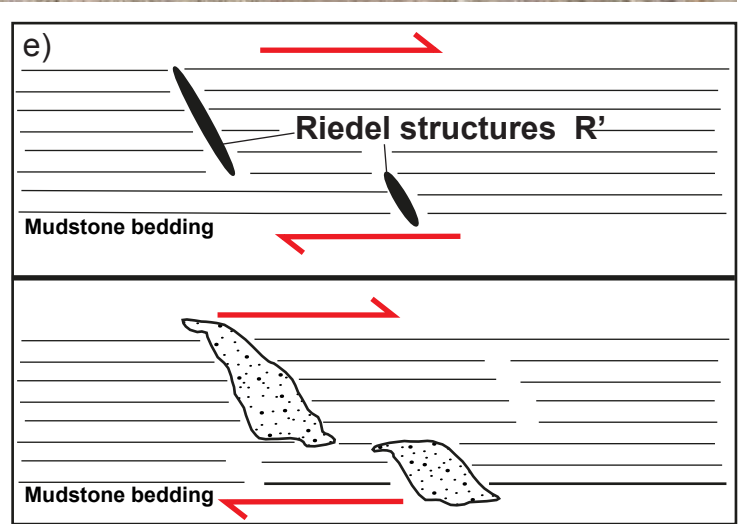
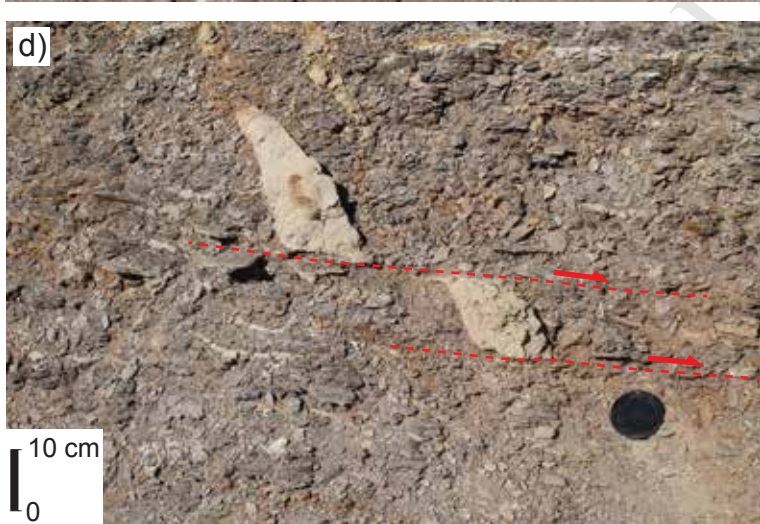
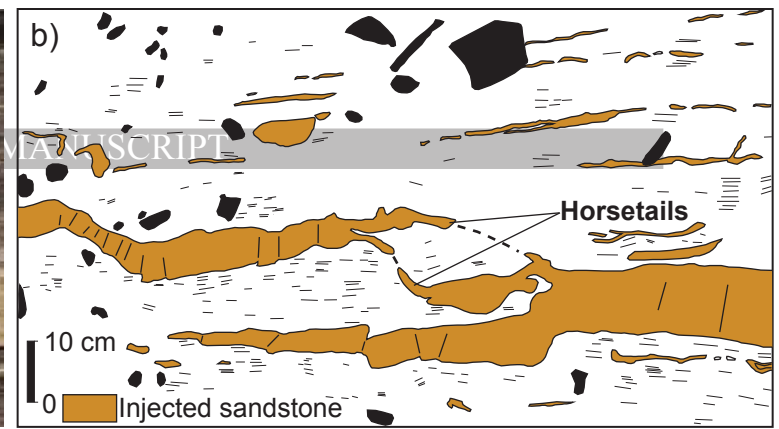
ESE

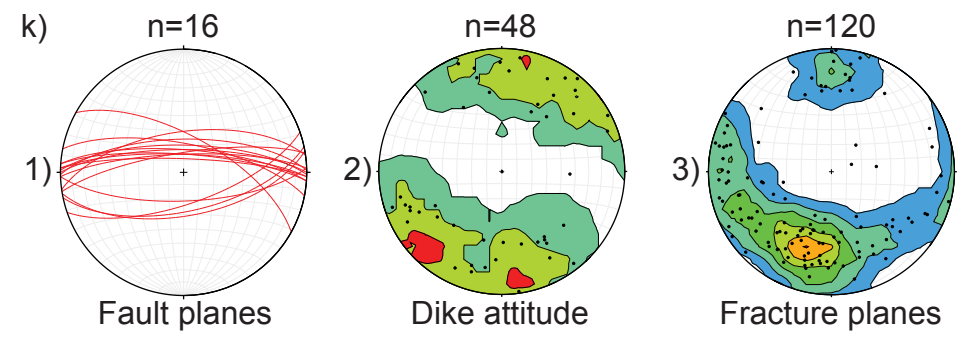
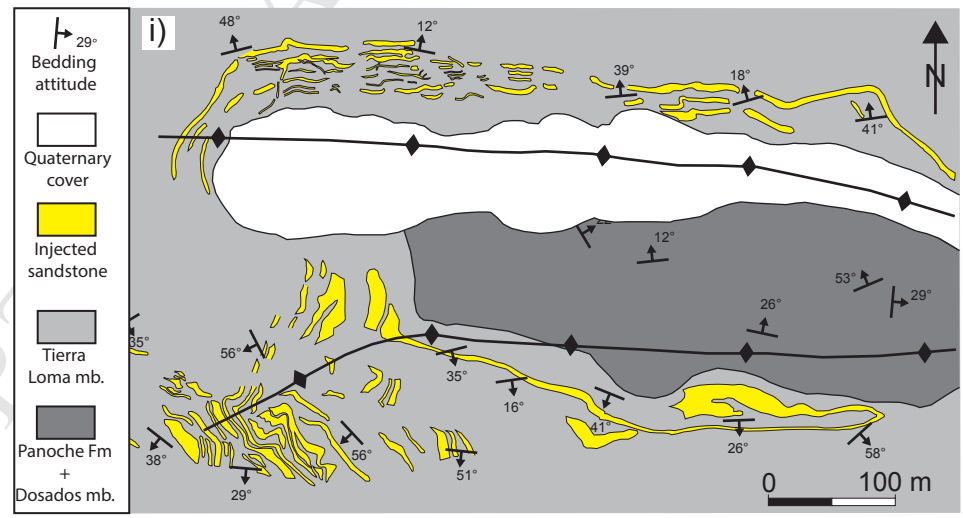
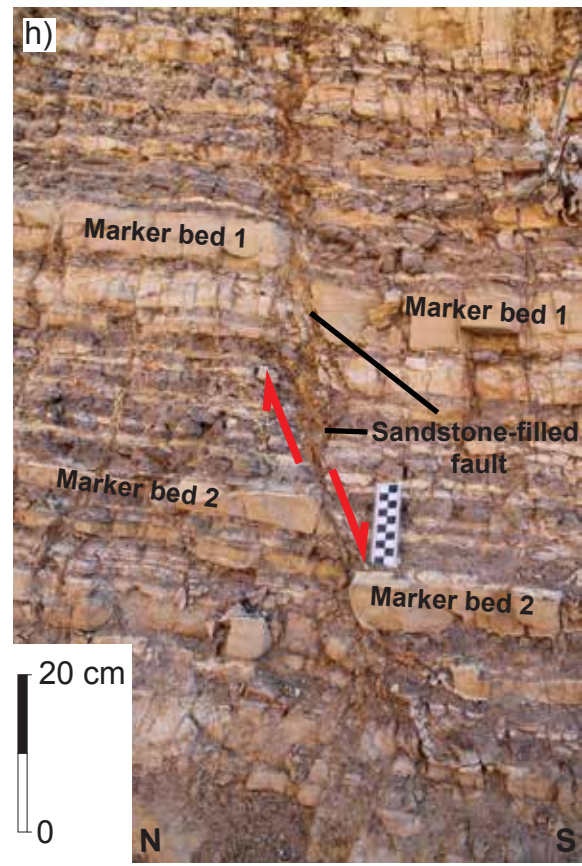
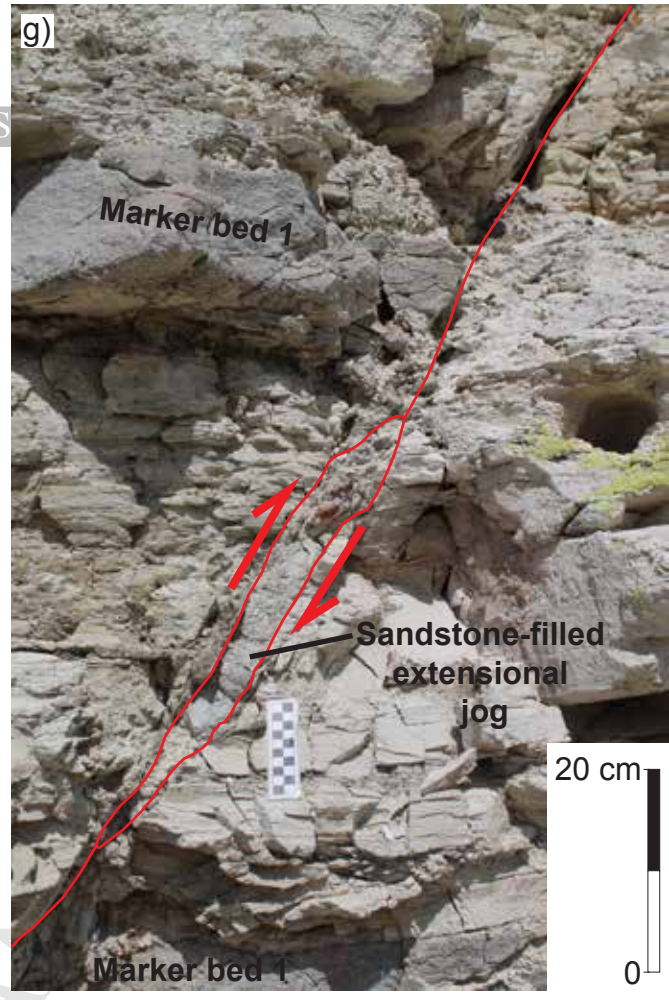
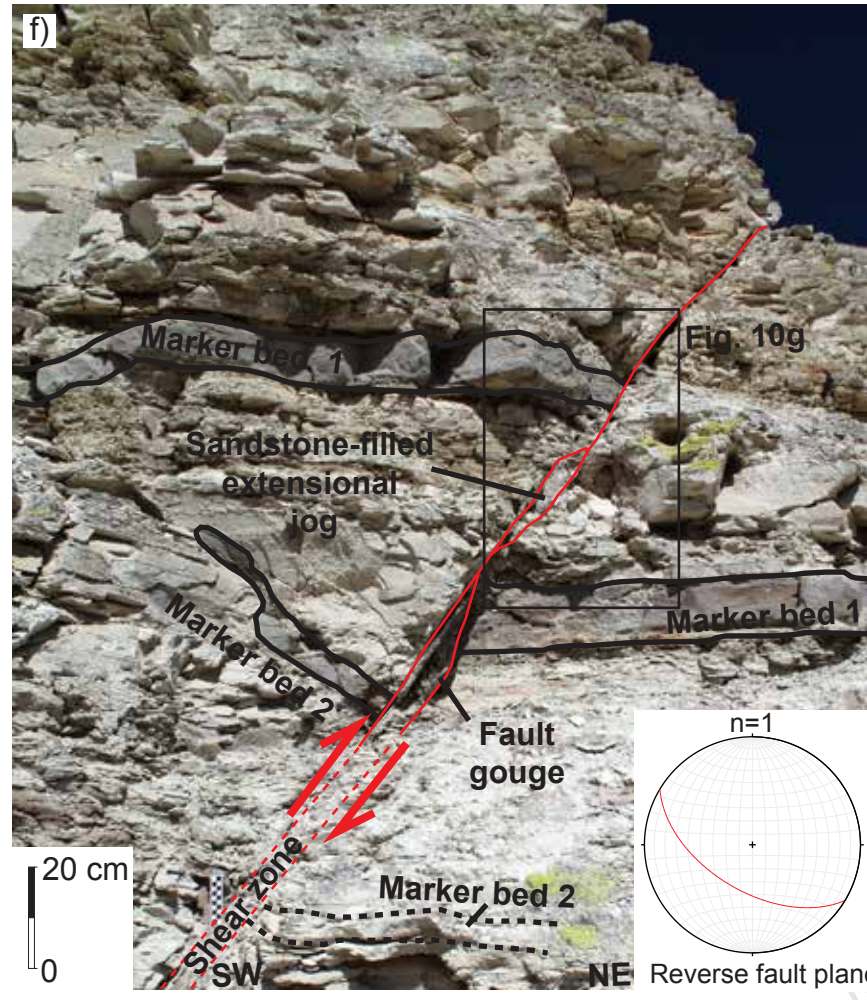


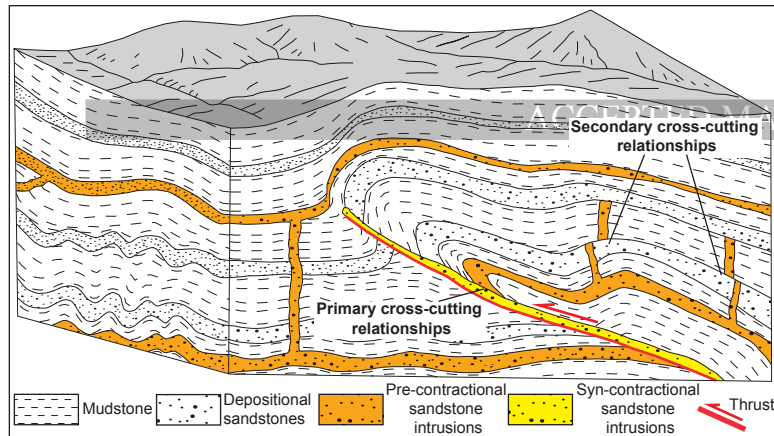
ACCEPTED MANUSCRIPT



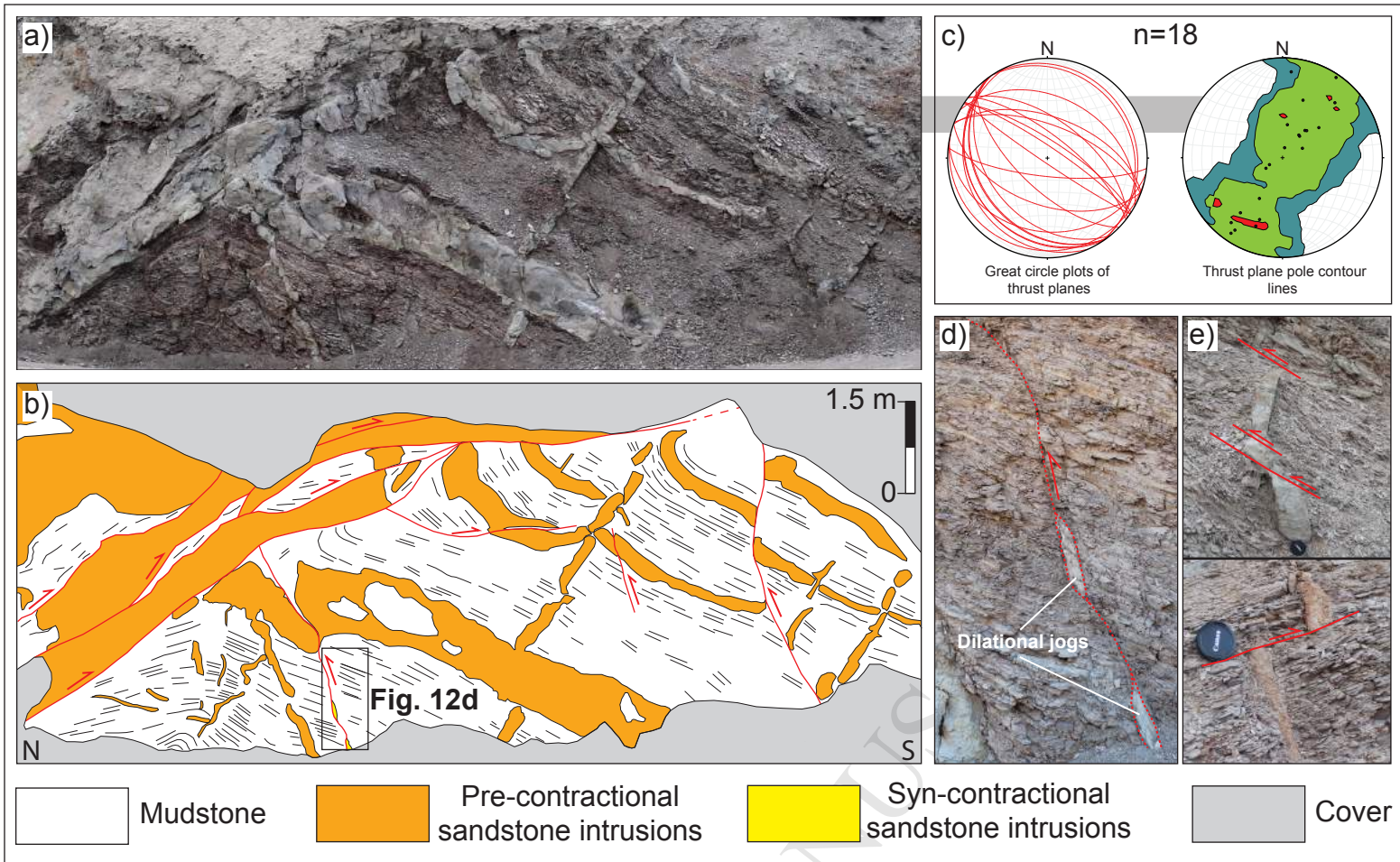
ACCEPTED MANUSCRIPT



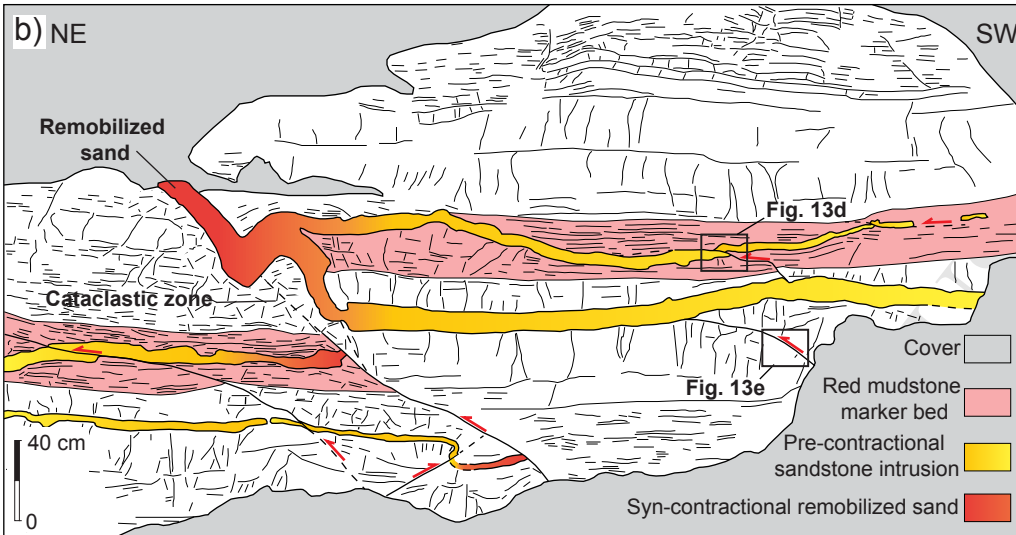
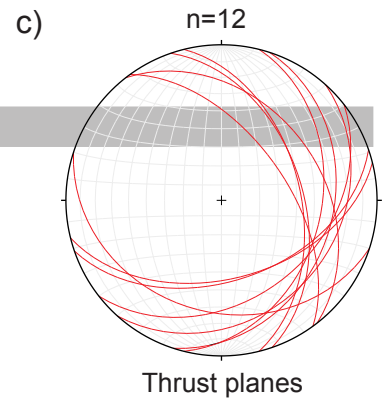




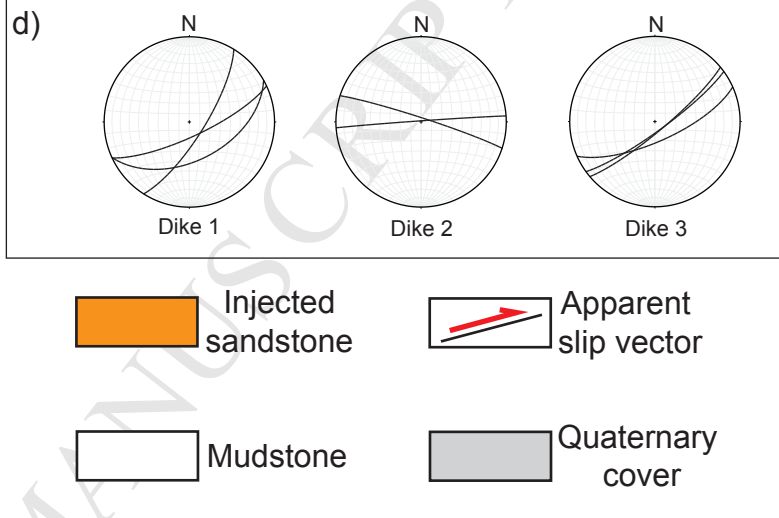
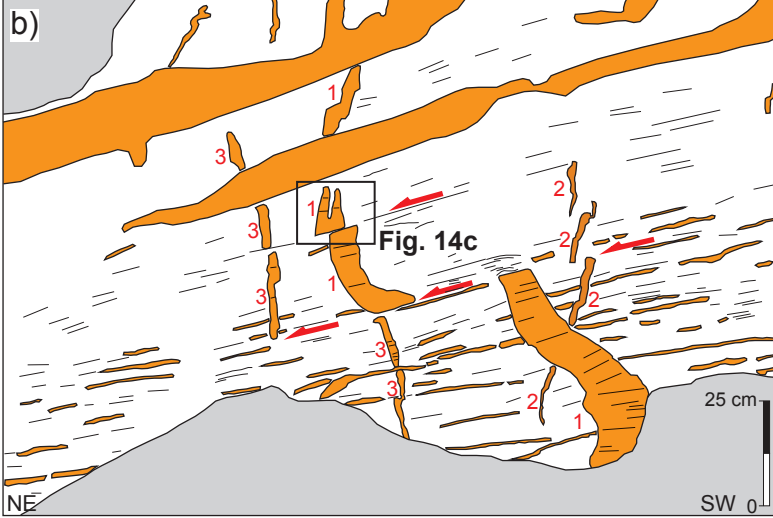
ACCEPTED MANUSCRIPT



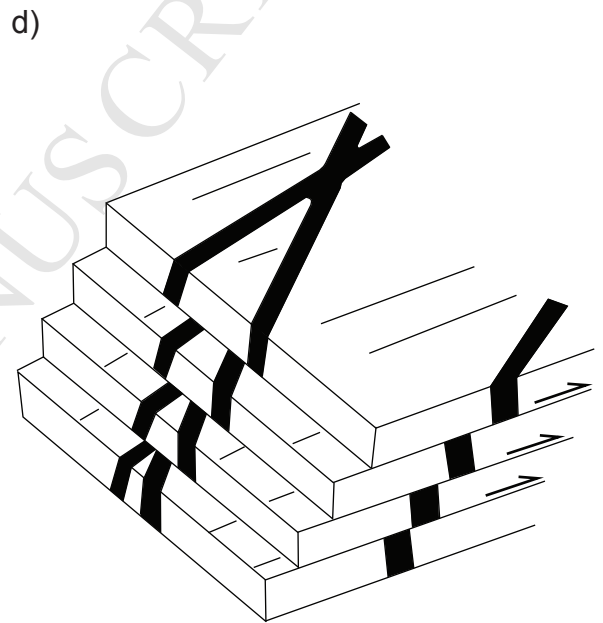
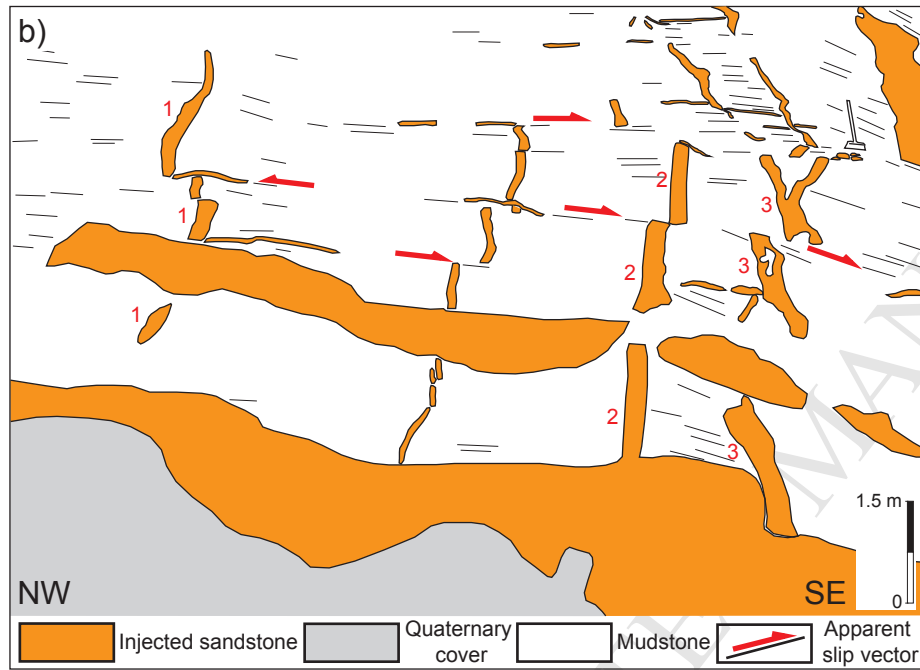
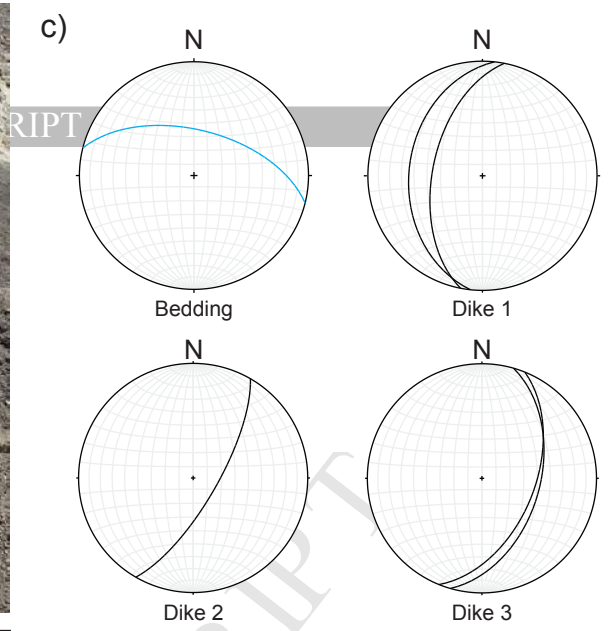
ACCEPTED MANUSCRIPT



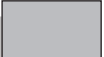
ACCEPTED MANUSCRIPT




ACCEPTED MANUSCRIPT

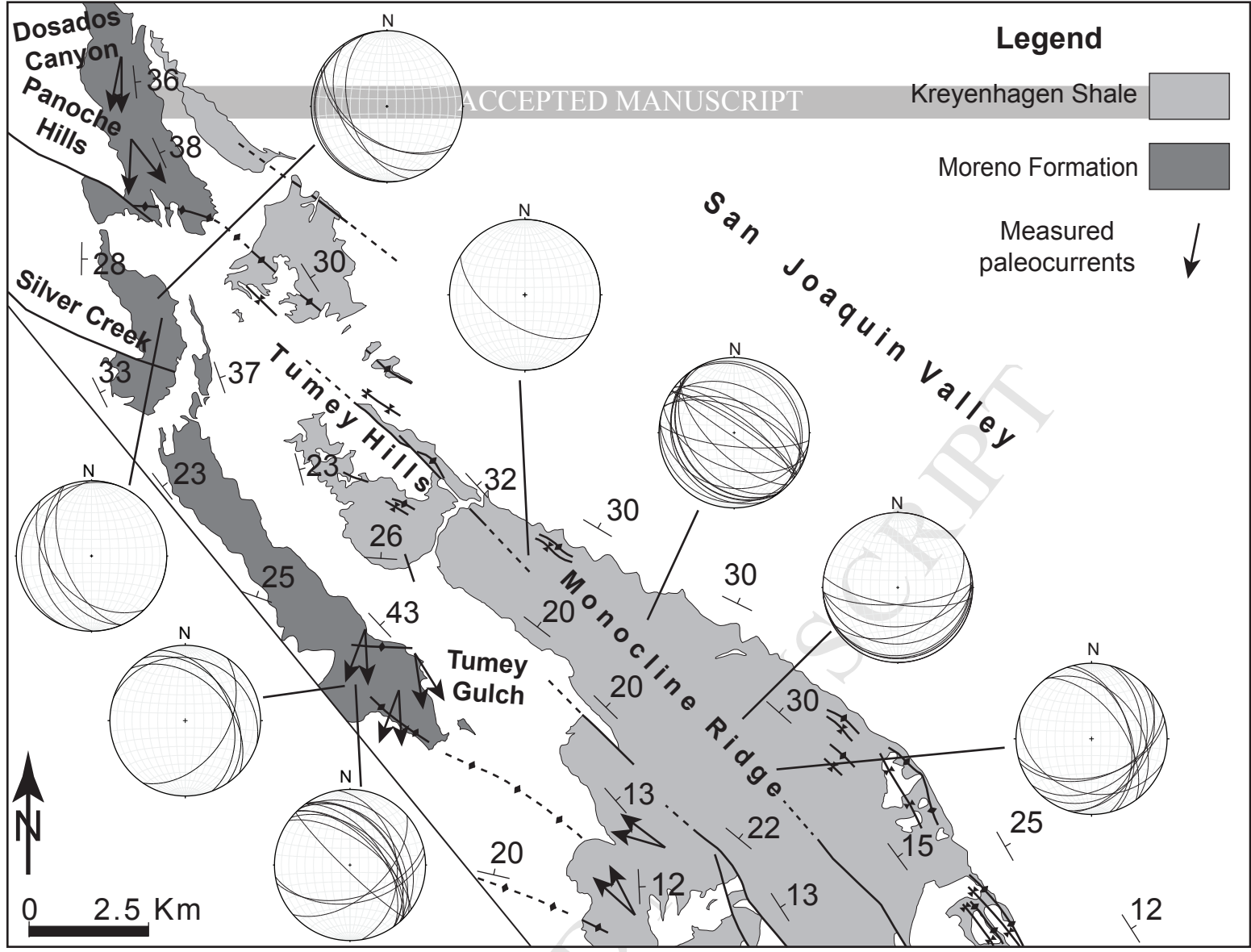


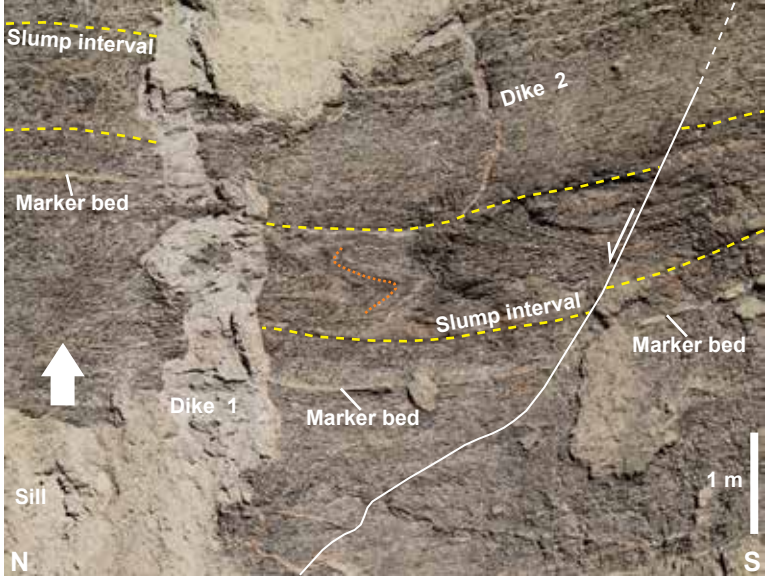
Legend

Kreyenhagen Shale 

Moreno Formation 

Measured paleocurrents 





ACCEPTED MANUSCRIPT

